



Impact of global change on coastal oxygen dynamics and risk of hypoxia

L. Meire^{1,2}, K. E. R. Soetaert¹, and F. J. R. Meysman^{1,3}

¹Department of Ecosystem Studies, Royal Netherlands Institute of Sea Research (NIOZ), Korringaweg 7, 4401 NT, Yerseke, the Netherlands

²Marine Biology Research group, University of Ghent (UGent), Krijgslaan 281 (S8), 9000 Ghent, Belgium

³Department of Analytical and Environmental Chemistry, Vrije Universiteit Brussel (VUB), Pleinlaan 2, 1050 Brussels, Belgium

Correspondence to: L. Meire (lorenz.meire@nioz.nl)

Received: 10 September 2012 – Published in Biogeosciences Discuss.: 29 October 2012

Revised: 27 February 2013 – Accepted: 13 March 2013 – Published: 19 April 2013

Abstract. Climate change and changing nutrient loadings are the two main aspects of global change that are linked to the increase in the prevalence of coastal hypoxia – the depletion of oxygen in the bottom waters of coastal areas. However, it remains uncertain how strongly these two drivers will each increase the risk of hypoxia over the next decades. Through model simulations we have investigated the relative influence of climate change and nutrient run-off on the bottom water oxygen dynamics in the Oyster Grounds, an area in the central North Sea experiencing summer stratification. Simulations were performed with a one-dimensional ecosystem model that couples hydrodynamics, pelagic biogeochemistry and sediment diagenesis. Climatological conditions for the North Sea over the next 100 yr were derived from a global-scale climate model. Our results indicate that changing climatological conditions will increase the risk of hypoxia. The bottom water oxygen concentration in late summer is predicted to decrease by 24 μM or 11.5 % in the year 2100. More intense stratification is the dominant factor responsible for this decrease (58 %), followed by the reduced solubility of oxygen at higher water temperature (27 %), while the remaining part could be attributed to enhanced metabolic rates in warmer bottom waters (15 %). Relative to these climate change effects, changes in nutrient runoff are also important and may even have a stronger impact on the bottom water oxygenation. Decreased nutrient loadings strongly decrease the probability of hypoxic events. This stresses the importance of continued eutrophication management in coastal areas, which could function as a mitigation tool to counteract the effects of rising temperatures.

1 Introduction

Coastal hypoxia refers to the depletion of oxygen in the bottom waters of coastal systems, and this phenomenon occurs when the consumption of oxygen outweighs the oxygen supply for a sufficiently long period (Diaz, 2001; Middelburg and Levin, 2009). Hypoxia is a natural phenomenon in fjords or basins with restricted water circulation (e.g. Black Sea, Santa Barbara Basin), or in shelf regions subject to the upwelling of oxygen-depleted and nutrient-rich subsurface water (e.g. North East Pacific, Namibian Shelf, Arabian Sea). Alongside this natural hypoxia there is strong evidence for a global increase in the frequency, extent, intensity and duration of coastal hypoxia linked to human activities (Diaz and Rosenberg, 2008). A recent survey shows a 5.5 % per year increase over the last three decades in the number of coastal sites with reported hypoxia (Vaquer-Sunyer and Duarte, 2008). Although this increase could partially reflect increased monitoring efforts, the prevalence of coastal hypoxia is clearly increasing as well.

Hypoxia has major consequences for the functioning of coastal ecosystems, as below a certain “hypoxia threshold”, marine organisms are exposed to a variety of stresses, which become lethal when the oxygen concentration becomes too low (Rabalais et al., 2010). A widely used reference level for coastal hypoxia is $\sim 63 \mu\text{M}$, although the actual threshold varies strongly between different faunal groups, with crustaceans and fish being the most sensitive (Vaquer-Sunyer and Duarte, 2008). Early stages of hypoxia are often missed until obvious signs, such as mass mortality of fish, indicate that

thresholds have been passed. Well-known examples of such “dead zones” include the Gulf of Mexico and the East China Sea, and in European waters, the Adriatic Sea, the German Bight, the Baltic Sea and the north western shelf of the Black Sea (Diaz and Rosenberg, 2008). Typically, coastal systems subject to hypoxia are also major fishery areas of strong economic interest (Diaz and Rosenberg, 2008). Until now, the formation of these dead zones has been primarily linked to coastal eutrophication fuelled by riverine import of fertilizers and atmospheric nitrogen deposition linked to the burning of fossil fuels. However, the combination of sustained eutrophication with future climate change could intensify hypoxia to new levels of ecosystem impacts (Conley et al., 2009).

For coastal management purposes it is crucially important to predict to what extent hypoxia will increase over the next 100 yr. To this end, one has to evaluate the two principal components of global change that are thought to strongly influence coastal hypoxia: climate change and nutrient runoff. Foremost, climate change will affect the concentration of oxygen in coastal waters in a number of ways. Oxygen is less soluble in warmer water, and hence an increase in global temperature will decrease the inventory of oxygen in coastal waters as well as the open ocean (Keeling et al., 2010). Higher temperatures will also intensify stratification, thereby reducing the downward oxygen supply to bottom waters and seafloor ecosystems (Keeling et al., 2010; Peña et al., 2010). Often climate change is also associated with a stronger hydrological cycle, and hence coastal areas with increased precipitation may experience stronger stratification, resulting in more intense hypoxia. Finally, higher seawater temperatures will enhance the respiratory and metabolic rates of organisms, thus stimulating the biological demand for oxygen (Conley et al., 2009). However, climate change may also counteract the future development of hypoxia by increasing both the intensity and frequency of summer storms, which may disrupt stratification and in this way ventilate the bottom waters (Rabalais et al., 2010). In addition to climate effects, the coastal zone is affected by increased nutrient delivery from land (Diaz, 2001). Human activity has greatly accelerated the flow of nutrients to estuaries and coastal ecosystems over the past half century, thus leading to increased primary production in the coastal zone. This results in a larger supply of organic material to deeper water layers and sediments, stimulating respiration in bottom waters (Conley et al., 2009; Diaz and Rosenberg, 2008). Such human-induced nutrient inputs have substantially affected the bottom water oxygenation in coastal ecosystems since the 1960s, strongly increasing the number of systems and the area in the coastal zone prone to hypoxia (Diaz and Rosenberg, 2008; Diaz, 2001; Zhang et al., 2010).

So a key question is what specific aspect of global change will dominate the future development of coastal hypoxia: a changing seasonal heating cycle (i.e. increased water temperatures), changes in storm frequency and intensity, or changes in human-induced nutrient inputs? To evaluate and

compare the effect of these different drivers, we performed a modelling study of the Oyster Grounds, a summer-stratified region in the central North Sea. At present, this region does not experience hypoxia (Greenwood et al., 2010; Queste et al., 2012), but in exceptional years, bottom water oxygen concentrations as low as 65 μM have been reported (Weston et al., 2008). Some studies have conjectured that climate change scenarios could bring the central North Sea to the brink of hypoxia (Weston et al., 2008), which would be detrimental to the rich bottom fauna in this area. In this study we performed simulations with a coupled physical–biogeochemical model to separately quantify the effect of changing climate forcings and nutrient loadings on the oxygen dynamics, comparing the current situation with the situation at the end of the twenty-first century.

2 Material and methods

2.1 Study area

The Oyster Grounds is a summer-stratified region in the central North Sea (54°30' N and 4°30' E) (Fig. 1). The area forms a large circular depression, at most 50 m deep, which is bordered by the shallower areas of the Dogger Bank, the German Bight and the southern North Sea. Currents and tides in the Oyster Grounds are weak (van der Molen, 2002), which leads to an increased deposition of fine sediment and organic material. As a result the sediment within the Oyster Grounds consists of muddy sand rich in organic matter (Boon et al., 1999; Neubacher et al., 2011). In the near future the Oyster Grounds area is scheduled to become a marine area protected because of its ecological richness (Offringa et al., 2004). So a proper assessment of the future risk of hypoxia in this region is vital.

One intriguing observation is the strong interannual variability in the oxygen concentration of the bottom water in late summer. Published oxygen minimum values vary from ~ 185 –220 μM in August 1976 (Postma and Rommets, 1984), ~ 203 μM and ~ 140 μM in the summer of 1988 and 1989, respectively (Peeters et al., 1995), 162 μM in July 2007 (Greenwood et al., 2010) to 180 μM in August 2010 (Queste et al., 2012). These oxygen concentrations are all well above the classical reference level for coastal hypoxia of ~ 63 μM . However, lower oxygen concentrations have also recently been reported. Boers (2005) reported 100 μM in September 2003, while in October 2003 (after an extremely warm summer), Weston et al. (2008) measured a bottom oxygen concentration of 65 μM in the centre of the Oyster Grounds. This latter value indicates that the area could be on the brink of hypoxia in exceptional years.

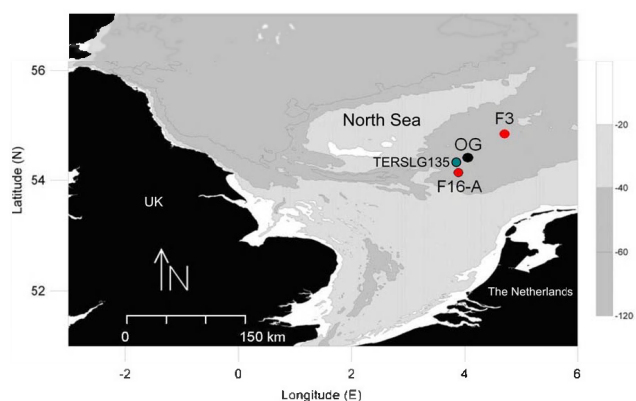


Fig. 1. Location of the CEFAS smartbuoy in the Oyster Grounds (OG, black dot) on a bathymetric map of the North Sea. The KNMI meteorological platforms (F16-A and F3) are also indicated on the map (red dots). The grey dot indicates the location of the Terschelling 135 (TERS LG135) Rijkswaterstaat monitoring point. Modified after Greenwood et al. (2010)

2.2 Geochemical data set

Continuous time series of temperature, chlorophyll *a* (chl *a*) concentration, turbidity and oxygen concentration were obtained at three different water depths (1 m, 35 m, 45 m) from CEFAS smartbuoys (Mills et al., 2003). Chlorophyll fluorescence was determined using a chlorophyll fluorometer (Sea-point Inc., USA) and turbidity with a turbidity meter (Sea-point Inc., USA) with a 1 Hz frequency. Measurements were recorded at a frequency of 1 Hz for temperature and conductivity using FSI CT sensors (Falmouth Scientific Inc., USA). Oxygen concentrations were determined at 5 Hz using an Aanderaa optode (AADI, Norway). More information on the moored instrumentation and processing can be found in Greenwood et al. (2010).

Daily averaged data are available for temperature, chl *a*, turbidity and oxygen at the water depths of 35 m and 45 m (from 21 April 2007 to 10 August 2008). At a water depth of 1 m, the dataset includes daily averaged measurements of the temperature, chl *a* and turbidity (from 1 January 2007 to 31 August 2008). In addition to the mooring data, discrete monthly data for surface water chlorophyll and oxygen concentrations over the period 2000 to 2010 were obtained from the Rijkswaterstaat monitoring programme and retrieved from the WaterBase database (<http://live.waterbase.nl/>; station Terschelling 135 km).

2.3 Model description

To describe the seasonal and long-term oxygen dynamics of the bottom water, we developed a coupled physical–biogeochemical model which describes the biogeochemical cycling of C, N and O₂ within both the water column and the sediment. This one-dimensional model consists of three

submodels, which respectively describe the water column physics, the pelagic ecosystem dynamics and the benthic biogeochemistry (Fig. 2). The water column physics model covers a 50 m deep water column, which is represented by an equidistant grid of 50 layers. The pelagic biogeochemical model has higher spatial resolution and consists of 100 equally spaced layers of 0.5 m thickness. The sediment biogeochemistry model covers a sediment depth of 25 cm and implements an uneven spatial grid to account for strong geochemical gradients near the sediment–water interface. The sediment grid consists of 100 layers, which have an increasing thickness from 1 mm near the sediment–water interface to 5 mm at a depth of 25 cm. The coupling between the three submodels is detailed in Fig. 2. Two different sets of dynamic model simulations were performed. The model was first calibrated on data from the year 2007. Using this calibrated parameter set, the model was subsequently run over the period 2000–2100.

2.3.1 Physical model of the water column

A one-dimensional k - ϵ turbulence closure model simulates the water column mixing and temperature dynamics (Gaspar et al., 1990; Soetaert et al., 2001). This model describes the dynamics of four state variables: the temperature (T ; °C), the water velocity in two horizontal directions (u , v ; m s⁻¹) and the turbulent kinetic energy (TKE; m² s⁻²). To simplify the model description, salinity is assumed constant throughout the water column, reflecting the idea that stratification is dominated by temperature gradients in the central North Sea (Ruardij et al., 1997; Greenwood et al., 2010). The energy balance regulates the temperature dynamics and accounts for heating due to solar radiation and vertical energy transport due to turbulence. The heat flux across the air–sea interface is calculated using a parameterization for short-wave incoming radiation, long-wave back radiation, and sensible and latent heat transfer. The Coriolis force, tidal forcings and turbulent exchange are taken into account in the momentum balance. At the air–sea interface, the momentum balance is forced using wind stress, while frictional stress due to currents operates at the sediment–water interface. All model equations and parameter values are listed in Tables 1, 2 and 3.

2.3.2 Pelagic biogeochemical model

The pelagic biogeochemical model is based upon an extended NPZD model formulation and uses a fixed Redfield stoichiometry to couple the nitrogen, carbon and oxygen cycles. The pelagic model includes seven state variables (all expressed in mmol m⁻³): ammonium (NH₄), nitrate (NO₃), phytoplankton (PHYTO), zooplankton (ZOO), detritus (DET), oxygen demand units (ODU) and oxygen (O₂). The biogeochemical reactions affecting these state variables are listed in Table 4 (Reactions 1–6). The associated

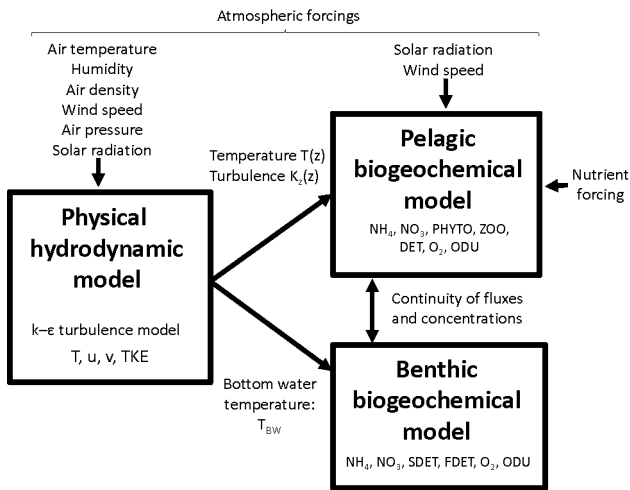


Fig. 2. The model consists of 3 submodels: a hydrodynamic $k-\epsilon$ model, a pelagic biogeochemical model and sediment biogeochemistry model. Atmospheric forcings drive the physical model. Water temperature (T) and turbulent mixing coefficient (K_z) are exported to the pelagic biogeochemical model, which is furthermore forced by solar radiation and wind speed. The bottom water temperature is exported to the benthic biogeochemical model. Fluxes of oxygen (O_2), nitrate (NO_3), ammonium (NH_4) and oxygen demand units (ODU) are exchanged across the sediment–water interface. Also deposition of organic material on the sediment is modelled which is split into fast (FDET) and slow (SDET) decaying detritus.

mass balance statements are listed in Table 5, while Table 8 shows the parameter values used in the pelagic model.

Primary production is assumed to be limited by nitrogen, as observed in many coastal systems (Neubacher et al., 2011; Suratman et al., 2008), including the Oyster Grounds (Weston et al., 2008). Primary production hence converts dissolved inorganic nitrogen (DIN) into phytoplankton biomass (PHYTO). DIN is further partitioned into ammonium and nitrate, where ammonium is the preferred nutrient during photosynthesis (this preferential uptake is modelled via the regulation factor α_{NH_4}). A conversion factor of $1 \mu\text{g chl } a$ per mmol N is used to calculate chlorophyll a from phytoplankton biomass. Phytoplankton is grazed upon by zooplankton (ZOO) using a functional type II dependence (Monod-type kinetics). Zooplankton mortality is modelled as a quadratic function of the zooplankton biomass. Phytoplankton mortality, zooplankton mortality and zooplankton faeces production all lead to the formation of detritus (DET). This detritus sinks through the water column (constant sinking speed w_{DET}), where it can be mineralized aerobically (consuming oxygen) or anaerobically producing oxygen demand units (ODU). ODU are a generic way of modelling the reduced compounds resulting from anaerobic organic matter mineralization. Phytoplankton also sinks through the water column with a constant sinking velocity (w_{PHYTO}).

Oxygen is supplied by reaeration through the air–sea interface. The air–sea exchange depends on the gradient between the actual oxygen concentration in the surface water and the saturating oxygen concentration (which is a function of the water temperature and salinity). The piston velocity (v_d) is calculated according to the formula of Wanninkhof and McGillis (1999) and depends quadratically on wind speed and the temperature. Oxygen is consumed in the water column by zooplankton respiration, oxic mineralization, nitrification and reoxidation of ODU.

The pelagic biogeochemical model is forced by solar radiation (affecting the light climate of primary production) and wind (affecting the air–sea exchange of oxygen). Water temperature and the turbulent mixing coefficient (K_z) are supplied as a function of water depth by the physical model (see *Physical Model*). The temperature dependence of biogeochemical reactions is implemented using a Q_{10} formulation, correcting the rates for the difference between the actual temperature T and a reference temperature T_{ref} (20°C). A Q_{10} formulation is the standard temperature response adopted in the OCMIP-type ocean biogeochemistry models (Marinov et al., 2010; Najjar et al., 2007). Over a century time scale, adaption of organisms or changes in community structure can occur, which may cause change in the apparent Q_{10} factor. However, such changes are difficult to quantify, and are not accounted for in the current model.

2.3.3 The benthic biogeochemical model

The sediment model is an adaptation of the OMEXDIA model originally developed by Soetaert et al. (1996a) and describes the sedimentary cycling of carbon, nitrogen and oxygen. The biogeochemical reactions of the sediment model are listed in Table 4 (Eqs. 4–7), the mass balances are shown in Table 7, while the model parameters are listed in Table 9. The model includes six state variables: two fractions of organic matter with different degradability (SDET and FDET), oxygen, nitrate, ammonium and ODU. Nitrogen is lost in the sediment through denitrification. Since anammox only accounts for 18% loss of nitrogen at the Oyster Grounds, the process is not included in the model (Neubacher et al., 2011). A bioturbation constant of $10 \text{ cm}^2 \text{ yr}^{-1}$ is adopted for the upper sediment layers reflecting the intense mixing activity observed in the Oyster Grounds (Birchenough et al., 2012). Porosity decreases exponentially with depth based on parameter values supplied in Neubacher et al. (2011). Sediment accretion is not taken into account, as for the Oyster Grounds it has been shown that sedimentation rates are low (Boon et al., 1999).

2.4 Atmospheric forcings

Our model simulations require suitable meteorological forcings at the air–sea interface. These include wind speed (m s^{-1}), atmospheric pressure (Pa), specific air humidity (dimensionless), air temperature ($^\circ\text{C}$), air density (kg m^{-3}) and

Table 1. Equations for the k - ϵ turbulence closure model. Table 2 lists the meaning of the state variables, output variables and forcing functions. The values of parameters are given in Table 3. The quantity z represents water depth.

State Variables	Conservation equations	Air–sea boundary	Sediment boundary
Temperature (T , °C)	$\frac{\partial T}{\partial t} = \frac{\partial}{\partial z} \left[K_z \frac{\partial T}{\partial z} \right] - \frac{1}{\rho_0 C_p} \frac{\partial I_z}{\partial z}$ $I_z = I_0 [p_{\text{long}} \exp(- (k_{\text{long}} + k_{\text{ext}})z) + (1 - p_{\text{long}}) \exp(- (k_{\text{short}} + k_{\text{ext}})z)]$	$-K_z \frac{\partial T}{\partial z} = \frac{(1 - 0.05) I_0}{\rho_0 C_p} + \frac{Q_e + Q_s + Q_b}{\rho_0 C_p}$	$K_z \frac{\partial T}{\partial z} = \frac{I_b}{\rho_0 C_p}$
Velocity in x , y (u , v , ms^{-1})	$\frac{\partial u}{\partial t} - f v = - \sum_{i=1}^2 A_x^i \sin\left(\frac{2\pi t - f_x^i}{\varphi^i}\right) + \frac{\partial}{\partial z} \left(K_m \frac{\partial u}{\partial z} \right)$ $\frac{\partial v}{\partial t} - f u = - \sum_{i=1}^2 A_y^i \sin\left(\frac{2\pi t - f_y^i}{\varphi^i}\right) + \frac{\partial}{\partial z} \left(K_m \frac{\partial v}{\partial z} \right)$ $f = 2 \times 7.292 \times 10^{-5} \sin\left(\frac{\text{Lat}}{360} \pi\right)$	$-K_m \frac{\partial u}{\partial z} = \frac{\rho_a}{\rho_0} \text{CD}_{10} W_{10} \cos(\theta_{10}) W_{10} $ $-K_m \frac{\partial v}{\partial z} = \frac{\rho_a}{\rho_0} \text{CD}_{10} W_{10} \sin(\theta_{10}) W_{10} $ $\text{CD}_{10} = \frac{(0.81 + 0.064 W_{10})}{1000}$	$-K_m \frac{\partial u}{\partial z} = r \sqrt{u_1^2 + v_1^2} u_1$ $-K_m \frac{\partial v}{\partial z} = r \sqrt{u_1^2 + v_1^2} v_1$ $u_1 = \frac{u_z}{1 + \frac{\sqrt{r}}{\kappa} \ln(z)}$
Turbulent kinetic energy (TKE, $\text{m}^2 \text{s}^{-2}$)	$\frac{\partial \text{TKE}}{\partial t} = K_m \left[\left(\frac{\partial u}{\partial z}\right)^2 + \left(\frac{\partial v}{\partial z}\right)^2 \right] - \frac{g}{\rho_0} K_z \frac{\partial \rho}{\partial z}$ $- C_e \frac{\text{TKE}^{3/2}}{l_e} + \frac{\partial}{\partial z} \left(K_e \frac{\partial \text{TKE}}{\partial z} \right)$ $K_m = \min(K_0, C_k l_k \sqrt{\text{TKE}} + \nu)$ $K_z = K_m \text{Pr}$ $K_e = K_m \text{Pr}$	$\text{TKE}_0 = C_w \frac{\rho_a}{\rho_0} \text{CD}_{10} (W_{10})^2$	$\text{TKE}_z = 4u_*^2$ $u_*^2 = r (u_1^2 + v_1^2)$

Table 2. State variables, output variables and forcing functions of the physical k - ϵ model.

Variables	Units	Description
State variables		
T	°C	Temperature
u	ms^{-1}	Horizontal velocity in x-direction
v	ms^{-1}	Horizontal velocity in y-direction
TKE	$\text{m}^2 \text{s}^{-2}$	Turbulent kinetic energy per unit mass
Output variables		
Q_e	Wm^{-2}	Latent heat flux
Q_s	Wm^{-2}	Sensible heat flux
Q_b	Wm^{-2}	Back radiation
CD_{10}	-	Surface drag coefficient
f	s^{-1}	Coriolis term
u_1	ms^{-1}	Velocity in x-direction at 1 m above the sediment
v_1	ms^{-1}	Velocity in y-direction at 1 m above the sediment
u_z	ms^{-1}	Velocity in middle of grid cell immediately above the bottom
K_z	$\text{m}^2 \text{s}^{-1}$	Turbulent diffusivity
K_e	$\text{m}^2 \text{s}^{-1}$	Turbulent mixing coefficient for turbulent kinetic energy
K_m	$\text{m}^2 \text{s}^{-1}$	Turbulent viscosity
I_z	Wm^{-2}	Solar radiation at a given water depth
I_b	Wm^{-2}	Solar radiation at the sediment–water interface
l_e	m	Length scale related to dissipation
l_k	m	Length scale related to mixing
Atmospheric forcings		
W_{10}	ms^{-1}	Wind speed, 10 m above the sea surface
θ_{10}	rad	Wind direction, 10 m above the sea surface
I_0	Wm^{-2}	Solar radiation at air–sea interface
I_b	Wm^{-2}	Solar radiation at sediment boundary

solar radiation (W m^{-2}). Solar radiation and wind speed are needed for both the hydrodynamic model and the pelagic ecosystem model; the other four forcings are exclusively used in the hydrodynamic model (Fig. 2). Meteorological

forcings for the period 2000 to 2100 were obtained from simulations of the ECHAM5/MPI-OM coupled climate model in the ESSENCE project (Ensemble SimulationS of Extreme weather events under Nonlinear Climate changeE) (Sterl et al., 2009). These ESSENCE simulations are global in coverage and include an ensemble of 16 different model runs for the SRES A1B greenhouse emission scenario. Simulated meteorological data were extracted from the ESSENCE output for the central North Sea ($55^\circ 1' 29'' \text{N}$, $3^\circ 45' \text{E}$), thus resulting in an ensemble of 16 different atmospheric forcings over the period 2000 to 2100. These forcings consist of 3-hourly averages, 2 to 10 m above the sea surface, except for the solar radiation data, which consist of daily averages. Figure 3 shows temperature and wind speed data from one of the 16 runs of the ESSENCE climate model.

In addition to the ESSENCE simulations, hourly meteorological data (wind speed, maximum wind speed, wind direction, air pressure, air temperature and relative humidity) were retrieved from two meteo platforms in the central North Sea: KNMI platform F16A ($54^\circ 12' \text{N}$, $4^\circ 02' \text{E}$) for the period 2006–2010 and from the KNMI platform F3 ($54^\circ 51' \text{N}$, $4^\circ 43' \text{E}$) for the period 1996–2010 (Fig. 1). These data were used to verify the quality of the atmospheric forcings extracted from the ESSENCE climate model. The artificial data generated from the 16 ESSENCE runs compares well with observed meteo data for the period 2007–2010. The observed temperature at the KNMI platforms F3 and F16a lies within the 95 % confidence interval of the daily averaged ESSENCE simulations (Fig. 3). The atmospheric temperature at the Oyster Grounds shows a clear seasonal cycle, with a winter minimum of 5°C and a summer maximum around 16°C (monthly averaged values over multiple years). The wind predicted by the ESSENCE simulations for the North Sea area is, however, slightly higher than the wind observed

Table 3. Parameter values of the physical k - ϵ model.

Symbol	Value	Quantity	Unit	Reference
k_{long}	1	Background attenuation coefficient for longer wavelength light (> 600 nm)	m^{-1}	Soetaert et al. (2001)
k_{short}	0.05	Background attenuation coefficient for shorter wavelength light	m^{-1}	Soetaert et al. (2001)
k_{ext}	0.063	Attenuation coefficient due to biota, detritus, sediment	m^{-1}	Soetaert et al. (2001)
p_{long}	0.4	Part of light with a long wavelength	–	Soetaert et al. (2001)
C_p	3994	Specific heat capacity of water	$\text{J kg}^{-1} \text{ dgC}^{-1}$	Soetaert et al. (2001)
C_W	4	Proportionality factor of windstress with surface TKE	–	Soetaert et al. (2001)
κ	0.4	Von Karman constant	–	Soetaert et al. (2001)
ν	1×10^{-6}	Kinematic viscosity	$\text{m}^2 \text{ s}^{-1}$	Soetaert et al. (2001)
K_0	1	Maximal vertical diffusivity/viscosity	$\text{m}^2 \text{ s}^{-1}$	Soetaert et al. (2001)
Pr	1	Turbulent Prandtl number	–	Soetaert et al. (2001)
g	9.81	Gravitational acceleration	ms^{-2}	Soetaert et al. (2001)
r	0.0025	Bottom quadratic friction coefficient	–	Soetaert et al. (2001)
ρ_0	1024	Reference density sea water	kg m^{-3}	Soetaert et al. (2001)
ρ_a	1.2	Reference density air	kg m^{-3}	Soetaert et al. (2001)
Parameters specific for the Oyster Grounds				
C_e	0.65	Proportionality factor between energy dissipation and TKE ^{3/2}	–	Calibrated
C_k	0.35	Proportionality factor between TKE and diffusivity coefficient	–	Calibrated
A_x^1	4.08×10^{-6}	M2 surface slope amplitude in E–W (x) direction	ms^{-2}	Data NIOZ
A_y^1	0	M2 surface slope amplitude in N–S (y) direction	ms^{-2}	Data NIOZ
A_x^2	1.22×10^{-6}	S2 surface slope amplitude in E–W (x) direction	ms^{-2}	Data NIOZ
A_y^2	0	S2 surface slope amplitude in N–S (y) direction	ms^{-2}	Data NIOZ
f_x^1	0	M2 surface slope phase in E–W (x) direction	s	Data NIOZ
f_y^1	0	M2 surface slope phase in N–S (y) direction	s	Data NIOZ
f_x^2	0	S2 surface slope phase in E–W (x) direction	s	Data NIOZ
f_y^2	0	S2 surface slope phase in N–S (y) direction	s	Data NIOZ
φ^1	44714	M2 surface slope period	s	Data NIOZ
φ^2	43200	S2 surface slope period	s	Data NIOZ
Lat	54.15	Latitude	° North	

Table 4. Reaction equations used in the pelagic (1–6) and benthic (4–7) model. The compounds that are included as state variable in the model are modelled are in bold. ODU denotes oxygen demands units and is expressed in $\mu\text{M O}_2$.

(1)	$106\text{CO}_2 + 106\text{H}_2\text{O} + 16\text{NH}_4^+ + \text{H}_3\text{PO}_4$	\rightarrow	$(\text{CH}_2\text{O})_{106}(\text{NH}_3)_{16}(\text{H}_3\text{PO}_4) + 106\text{O}_2 + 16\text{H}^+$
(2)	$106\text{CO}_2 + 122\text{H}_2\text{O} + 16\text{NO}_3^- + 16\text{H}^+ + \text{H}_3\text{PO}_4$	\rightarrow	$(\text{CH}_2\text{O})_{106}(\text{NH}_3)_{16}(\text{H}_3\text{PO}_4) + 138\text{O}_2$
(3)	$\text{NH}_4^+ + 2\text{O}_2$	\rightarrow	$\text{NO}_3^- + \text{H}_2\text{O} + 2\text{H}^+$
(4)	$(\text{CH}_2\text{O})_{106}(\text{NH}_3)_{16}(\text{H}_3\text{PO}_4) + 106\text{O}_2 + 16\text{H}^+$	\rightarrow	$106\text{CO}_2 + 16\text{NH}_4^+ + \text{H}_3\text{PO}_4 + 106\text{H}_2\text{O}$
(5)	$(\text{CH}_2\text{O})_{106}(\text{NH}_3)_{16}(\text{H}_3\text{PO}_4) + \text{an oxidant}$	\rightarrow	$106\text{CO}_2 + 16\text{NH}_4^+ + \text{H}_3\text{PO}_4 + 106\text{ODU} + 106\text{H}_2\text{O}$
(6)	$\text{ODU} + \text{O}_2$	\rightarrow	oxidation products
(7)	$(\text{CH}_2\text{O})_{106}(\text{NH}_3)_{16}(\text{H}_3\text{PO}_4) + 100.8\text{H}^+ + 0.8 \times 106\text{NO}_3^-$	\rightarrow	$106\text{CO}_2 + 16\text{NH}_4^+ + 0.4 \times 106\text{N}_2 + \text{H}_3\text{PO}_4 + 1.4 \times 106\text{H}_2\text{O}$

on the KNMI meteo platforms (9 %). The wind speed of the ESSENCE simulations is therefore corrected by this factor so that the monitored wind speed lies within the 95 % confidence interval of the ESSENCE wind speed simulations. The wind prevailingly comes from the south-west and the yearly average wind speed is around 8 m s^{-1} (lowest in summer 6 m s^{-1} ; and highest in winter 10 m s^{-1}). The similarity between measured meteo data (KNMI) and the output of the ESSENCE climate simulation gives confidence in the

use of the ESSENCE synthetic meteo data as atmospheric forcings of the model, at least for the present-day conditions. The correctness of the predicted atmospheric forcings at the end of the 21st century will depend both on the accuracy of the ESSENCE climate model as well as on how SRES A1B scenario captures the true evolution in greenhouse gas emissions.

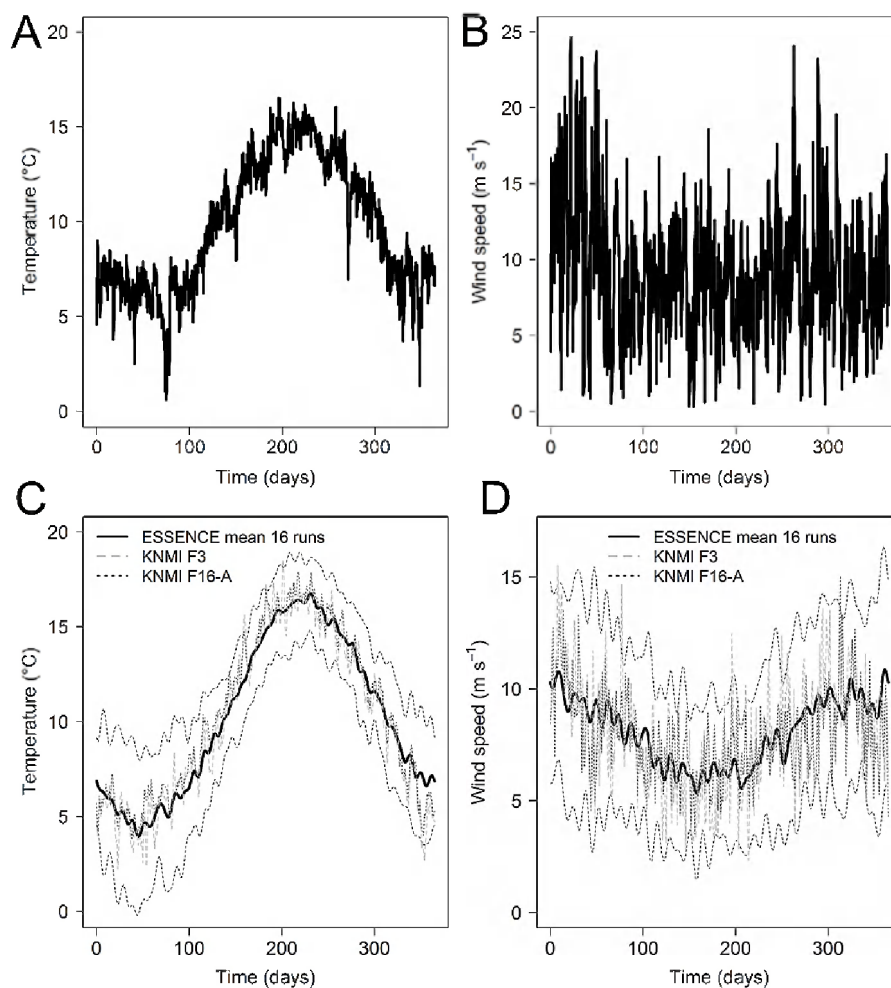


Fig. 3. Hourly temperature (A) and wind (B) data generated by the ESSENCE climate model (simulation run 2 for year 2010). Bottom panel shows a comparison between the simulations of the ESSENCE simulations (mean of 16 different simulation runs) (black solid line) and data from the F3 (dark grey solid line) and F16 (light grey solid line) station in the North Sea for the daily averaged temperature (C) and daily averaged wind speed (D) for the period 2007–2010. The 95 % confidence interval of the ESSENCE simulations is indicated with the black dotted line.

2.5 Nutrient forcings

The inclusion of sedimentary denitrification implies that there is an overall sink of nitrogen in the coupled pelagic-benthic model. If left uncompensated this leads to a gradual depletion of the nitrogen pool, and hence a (unacceptable) drift in the dynamic simulations. To retain a constant nitrogen pool, we compensated the loss of nitrogen by denitrification at each time step by a matching input flux of NH_4 to the uppermost pelagic compartment (Soetaert and Middelburg, 2009). This procedure implies that the size of the initial nitrogen pool in the model fully determines the nutrient loading imposed upon the model. This nutrient loading was not dynamically adapted in the simulations as we did not have reliable scenarios of how this nutrient loading will change over the simulation period 2000–2100. Instead, we

examined the effect of different nutrient loadings on hypoxia by performing simulations over the period 2000–2100 with different initial nitrogen pools, and thus simulating different nutrient loadings.

To constrain the present-day nutrient loading, the size of the nitrogen pool was estimated from the total dissolved nitrogen concentrations (TDN) in the surface water at the Oyster Grounds in the winter time (fully mixed water column). To this end, TDN data from a long-term water quality monitoring programme (WaterBase, station Terschelling 135) were averaged over the period 2000 to 2010, resulting in a ten-year average value of 11 mmol N m^{-3} and a range of 6 to 20 mmol N m^{-3} .

2.6 Model calibration

The majority of the parameters values were fixed a priori based on information from the available literature (Tables 1, 2 and 3). Tidal amplitudes and the phase of the M2 and S2 tides at the Oyster Grounds were based on data provided by P. Ruardij (personal communication, 2011). For a limited set of model parameters, the value could not be fixed a priori. To arrive at suitable values, we performed calibration simulations for the year 2007, where the model was fitted to the high-resolution CEFAS time series data over 2007. Ensemble results of the model forced by the 16 different ESSENCE simulations were compared with the CEFAS mooring data. The hydrodynamic model was first calibrated, and to this end we used the daily temperature data over 2007 at 1, 35 and 45 m water depth. Subsequently, we calibrated the coupled benthic–pelagic biogeochemical model by comparing the model output to several data sets (Fig. 5): (1) the chlorophyll *a* concentration as measured by the CEFAS buoy in the surface layer (1 m), (2) the dissolved oxygen concentration as measured by the CEFAS buoy at a depth of 35 and 45 m, and (3) the monthly water quality data of Rijkswaterstaat (also indicated in Fig. 5). Due to the high resolution of the CEFAS data, calibration was primarily focused on this mooring dataset. Parameter values were optimized by manual tuning.

2.7 Numerical solution

To assess the prevalence of lower bottom oxygen concentrations in the Oyster Grounds within the next 100 yr, we performed time-dependent simulations of the coupled model over the time period 2000–2100. These transient simulations were performed in an offline mode, where the simulation of the hydrodynamic model preceded that of the pelagic and benthic biogeochemical models. Two output variables from the physical model (water temperature T , turbulent mixing coefficient K_z) were stored as daily averaged values at each water depth, and were subsequently used as forcing functions in the pelagic (T , K_z) and benthic (T_{bw}) biogeochemical models (Fig. 2). The bottom water temperature T_{bw} imposed upon the sediment model was that of the lowest grid cell in the water column model; we assumed no temperature gradient in the sediment.

The coupling between the benthic and pelagic biogeochemical models was online and two-directional. Organic material sinking from the water column provided an input flux of detritus to the sediment. This flux was split into two pools FDET and SDET (representing fast and slow decaying organic matter) using a fixed ratio. Bottom water concentrations of oxygen, nitrate, ammonium and ODU from the pelagic model were used as upper boundary conditions in the sediment model. At the same time, fluxes across the sediment water interface were calculated by the sediment model, which were imposed as boundary conditions on the lower grid cell of the pelagic model.

All model equations were coded in FORTRAN routines that were embedded as DLL files within scripts in the programming language R (R Core Team, 2012). The solution of the coupled model was done using the R packages rootSolve (Soetaert and Herman, 2009) and deSolve (Soetaert et al., 2010). Details on solution and spin-up (i.e. to arrive at an initial steady state without model drift) can be found in Soetaert and Middelburg (2009) for the coupled pelagic–benthic model and in Soetaert et al. (2001) for the hydrodynamic model. Post-processing of model results and the generation of graphs was also done in the programming language R (R Core Team, 2012). It took about 2.5 min to run 1 yr of the full model (physical and biogeochemical model) on a 2.2 GHz personal computer.

3 Results and discussion

3.1 Model calibration

Stratification plays a critical role in the occurrence of hypoxia, and therefore it is essential to be able to accurately simulate the water column physics. To calibrate the physical model two parameters related to the dissipation rate (C_e) and the proportionality between TKE and eddy diffusivity coefficients (C_k) were tuned (Table 3). These parameters typically range between 0.1 and 0.5 for C_k , and between 0.1 and 0.7 for C_e (Gaspar et al., 1990; Soetaert et al., 2001). Several runs were performed using different parameter sets, and results were compared with the measured water temperatures at 1, 35 and 45 m water depths (CEFAS buoy dataset). The values $C_e = 0.65$ and $C_k = 0.35$ provided the best fit to the available data.

In the calibration of the coupled benthic–pelagic model, the correct simulation of both the timing and magnitude of the phytoplankton spring bloom is crucial. This was done by tuning the parameters: I_{opt} , $d_{\text{PHYTO-max}}$, $d_{\text{ZOO-max}}$, r_{ZOO} and g_{max} . The calibrated values of these parameters are listed in Table 8.

3.2 Present situation in the Oyster Grounds

After calibration, the model suitably describes the present-day ecosystem dynamics in the Oyster Grounds (Figs. 4 and 5 compare the model simulation output to observational data over the period 2007–2008). From November to the end of March, the water column is well mixed due to intensive wind-induced turbulence (Fig. 8). Consequently, the water temperature is uniform over the entire 50 m deep water column during this period. Water temperature is lowest in February and March, and starts to increase at the end of March due to higher solar radiation and higher air temperatures. In combination with lower wind speeds, this leads to the development of a stratified layer at the beginning of April (Greenwood et al., 2010; Ruardij et al., 1997). The water column remains stratified during summer, with the largest

Table 5. Mass balance equations of the pelagic ecosystem model. The state variables are in bold. The quantity z represents the depth in the water column. Oxidic mineralization (OxMin), anoxic mineralization (AnoxMin), net primary production (NPP), NH_4 fraction taken up in NPP (α_{NH_4}), nitrification (Nit), respiration (Resp), mortality (Mort), oxidation of oxygen demand units (ODU oxid).

$$\begin{aligned}
 \frac{\partial \text{NH}_4}{\partial t} &= \frac{\partial}{\partial z} \left[K_z \frac{\partial \text{NH}_4}{\partial z} \right] + \text{OxMin} + \text{AnoxMin} - \alpha_{\text{NH}_4} \text{NPP} - \text{Nit}_{\text{ZOO}} + \text{Resp}_{\text{ZOO}} \\
 \frac{\partial \text{NO}_3}{\partial t} &= \frac{\partial}{\partial z} \left[K_z \frac{\partial \text{NO}_3}{\partial z} \right] - (1 - \alpha_{\text{NH}_4}) \text{NPP} + \text{Nit} \\
 \frac{\partial \text{PHYTO}}{\partial t} &= \frac{\partial}{\partial z} \left[K_z \frac{\partial \text{PHYTO}}{\partial z} \right] - w_{\text{PHYTO}} \frac{\partial \text{PHYTO}}{\partial z} + \text{NPP} - \text{Grazing} - \text{Mort}_{\text{PHYTO}} \\
 \frac{\partial \text{ZOO}}{\partial t} &= \frac{\partial}{\partial z} \left[K_z \frac{\partial \text{ZOO}}{\partial z} \right] + q_{\text{zoo}} \text{Grazing} - \text{Mort}_{\text{ZOO}} - \text{Resp}_{\text{ZOO}} \\
 \frac{\partial \text{DET}}{\partial t} &= \frac{\partial}{\partial z} \left[K_z \frac{\partial \text{DET}}{\partial z} \right] - w_{\text{DET}} \frac{\partial \text{DET}}{\partial z} + (1 - q_{\text{zoo}}) \text{grazing} + \text{Mort}_{\text{ZOO}} + \text{Mort}_{\text{PHYTO}} - \text{OxMin} \\
 &\quad - \text{AnoxMin} \\
 \frac{\partial \text{O}_2}{\partial t} &= \frac{\partial}{\partial z} \left[K_z \frac{\partial \text{O}_2}{\partial z} \right] + \left(\gamma_{\text{O}_2}^{\text{NH}_4} \alpha_{\text{NH}_4} + \gamma_{\text{O}_2}^{\text{NO}_3} (1 - \alpha_{\text{NH}_4}) \right) \text{NPP} - \text{OxMin} - 2\text{Nit} - \gamma_{\text{O}_2}^{\text{N}} \text{Resp}_{\text{ZOO}} \\
 &\quad - \text{ODU}_{\text{oxid}} \\
 \frac{\partial \text{ODU}}{\partial t} &= \frac{\partial}{\partial z} \left[K_z \frac{\partial \text{ODU}}{\partial z} \right] + \text{AnoxMin} - \text{ODU}_{\text{oxid}}
 \end{aligned}$$

Table 6. Rate expressions of the pelagic ecosystem model, the state variables are in bold. Piston velocity (v_d), air–sea exchange (ASE), Schmidt number (Sc), wind speed at 10 m (u_{10}).

NPP	$= \mu_{\text{max}} f(T) \min(f(I), f(\text{DIN})) \text{PHYTO}$	(1)
$f(T)$	$= Q_{10}^{\left(\frac{T - T_{\text{ref}}}{10}\right)}$	(2)
$f(I)$	$= \tanh\left(\frac{I(z, t)}{I_{\text{opt}}}\right)$	(3)
$I(z, t)$	$= I_0(t) \exp(-k_w + k_p \text{PHYTO}) z$	(4)
$f(\text{DIN})$	$= \frac{\text{NO}_3}{\text{NO}_3 + K_{\text{SNO}_3}} e^{-\psi \text{NH}_4} + \frac{\text{NH}_4}{\text{NH}_4 + K_{\text{SNH}_4}}$	(5)
α_{NH_4}	$= \frac{f(\text{DIN}) \text{NH}_4 + K_{\text{SNH}_4}}{\text{NH}_4 + K_{\text{SNH}_4}}$	(6)
$\text{Mort}_{\text{PHYTO}}$	$= m_{\text{PHYTO}} f(T) \text{PHYTO}$	(7)
Grazing	$= g_{\text{max}} f(T) \frac{\text{PHYTO}}{\text{PHYTO} + K_{\text{SPHYTO}}} \text{ZOO}$	(8)
Mort_{ZOO}	$= m_{\text{ZOO}} f(T) \text{ZOO}^2$	(9)
Resp_{ZOO}	$= r_{\text{ZOO}} f(T) \text{ZOO}$	(10)
OxMin	$= r_{\text{min}} f(T) \frac{\text{O}_2}{\text{O}_2 + K_{\text{SO}_2}} \text{DET}$	(11)
AnoxMin	$= r_{\text{min}} f(T) \left(1 - \frac{\text{O}_2}{\text{O}_2 + K_{\text{SO}_2}}\right) \text{DET}$	(12)
Nit	$= r_{\text{nit}} f(T) \frac{\text{O}_2}{\text{O}_2 + K_{\text{SO}_2}} \text{NH}_4$	(13)
ODU oxid	$= r_{\text{ODU}} f(T) \frac{\text{O}_2}{\text{O}_2 + K_{\text{SO}_2}} \text{ODU}$	(14)
ASE	$= v_d (\text{O}_2^{\text{sat}} - \text{O}_2)$	(15)
v_d	$= 0.0283 u_{10}^3 (Sc/660)^{-1/2}$	(16)

difference between surface and bottom temperatures occurring at the end of July. In early autumn, stratification is broken due to increased wind speeds and decreased heating in the surface water layer. This breakdown of stratification occurs on average at the end of September and is followed by

a slow cooling of the homogenized water column during the winter (Greenwood et al., 2010; Ruardij et al., 1997).

The physical conditions strongly influence the ecosystem dynamics in the Oyster Grounds. Upon the onset of stratification, phytoplankton blooms until nutrients are depleted in the surface layer. The maximum phytoplankton concentration occurs at the beginning of April (day 100). Our simulation of phytoplankton net primary production (NPP) over 2007 provided $\sim 2.1 \text{ mol N m}^{-2} \text{ yr}^{-1}$, corresponding to a yearly carbon fixation of $\sim 14 \text{ mol C m}^{-2} \text{ yr}^{-1}$ ($\sim 170 \text{ g C m}^{-2} \text{ yr}^{-1}$). This result lies well within the (broad) range of NPP estimates from field studies at the Oyster Grounds and model simulations, which vary between 100 and $250 \text{ g C m}^{-2} \text{ yr}^{-1}$ (Gieskes and Kraay, 1984; Joint and Pomroy, 1993; Luff and Moll, 2004; Moll, 1998; Skogen and Moll, 2000). The grazing of the phytoplankton bloom by zooplankton leads to high production of detritus. A large fraction of this detritus and part of the phytoplankton bloom sinks out to the bottom layers, where this organic material is mineralized.

The combination of suitable physical (presence of stratification) and biological conditions (high primary production, resulting in detritus export to the bottom layers and associated oxygen consumption) leads to the observed decrease in the bottom water oxygen in the Oyster Grounds (Figs. 5 and 9) (Greenwood et al., 2010), which is suitably captured by our model simulations. In summer of 2007, the observed bottom water O_2 concentration drops to $\sim 180 \mu\text{M}$ (Fig. 5b). Using the 16 different ESSENCE meteo simulations of 2007, the minimum oxygen concentration in summer at the bottom varies over a range of $60 \mu\text{M}$, stressing the importance of atmospheric forcings (e.g. the timing of the break-up of stratification due to autumn storms).

Table 7. Model equations incorporated in the benthic biogeochemical model. State variables are in bold. The quantity z represents the depth into the sediment. Bottom water temperature (T_{BW}), Oxidic mineralisation (OxMin), anoxic mineralization (AnoxMin), nitrification (Nit), denitrification (Denit), oxidation of oxygen demand units (ODU oxid).

For a rapidly ($i = 1$) and slowly ($i = 2$) decaying carbon fraction

$$\Sigma = \frac{O_2}{O_2 + K_{SO_2}} + \frac{NO_3}{NO_3 + K_{SNO_3}} \left(1 - \frac{O_2}{O_2 + K_{in}^{Denit}} \right) + \left(1 - \frac{O_2}{O_2 + K_{in}^{Anox\ min}} \right) \left(1 - \frac{NO_3}{NO_3 + K_{in}^{Anox\ min}} \right)$$

$$OxMin = \sum_{i=1}^2 \left[r_i \mathbf{DET}_i f(T_{BW}) \frac{O_2}{O_2 + K_{SO_2}} \frac{1}{\Sigma} \right]$$

$$Denit = \sum_{i=1}^2 \left[r_i \mathbf{DET}_i f(T_{BW}) \frac{NO_3}{NO_3 + K_{SNO_3}} \left(1 - \frac{O_2}{O_2 + K_{in}^{Denit}} \right) \frac{1}{\Sigma} \right]$$

$$AnoxMin = \sum_{i=1}^2 \left[r_i \mathbf{DET}_i f(T_{BW}) \left(1 - \frac{O_2}{O_2 + K_{in}^{Anox\ min}} \right) \left(1 - \frac{NO_3}{NO_3 + K_{in}^{Anox\ min}} \right) \frac{1}{\Sigma} \right]$$

$$Nit = r_{nit} f(T_{BW}) \frac{O_2}{O_2 + K_{SO_2}^{nit}} \mathbf{NH}_4$$

$$ODU\ oxid = r_{ODU} f(T_{BW}) \frac{O_2}{O_2 + K_{SO_2}^{ODU}} \mathbf{ODU}$$

$$\frac{d\mathbf{DET}_i}{dt} = \frac{\partial}{\partial z} \left[D_b(z) \frac{\partial \mathbf{DET}_i}{\partial z} \right] - r_i f(T_{BW}) \mathbf{DET}_i$$

$$\frac{dO_2}{dt} = \frac{\partial}{\partial z} \left[D_s^{O_2} \frac{\partial O_2}{\partial z} \right] - \frac{1 - \phi(z)}{\phi(z)} OxMin - 2Nit - ODU\ oxid$$

$$\frac{d\mathbf{NH}_4}{dt} = \frac{\partial}{\partial z} \left[\frac{D_s^{NH_4}}{1 + \mathbf{NH}_{4ads}} \frac{\partial \mathbf{NH}_4}{\partial z} \right] + \frac{1 - \phi(z)}{\phi(z)} \gamma_{OC}^N \frac{[OxMin + Denit + AnoxMin]}{1 + \mathbf{NH}_{4ads}} - \frac{Nit}{1 + \mathbf{NH}_{4ads}}$$

$$\frac{dNO_3}{dt} = \frac{\partial}{\partial z} \left[D_s^{NO_3} \frac{\partial NO_3}{\partial z} \right] - 0.8 \frac{1 - \phi(z)}{\phi(z)} Denit + Nit$$

$$\frac{d\mathbf{ODU}}{dt} = \frac{\partial}{\partial z} \left[D_s^{ODU} \frac{\partial \mathbf{ODU}}{\partial z} \right] + \frac{1 - \phi(z)}{\phi(z)} AnoxMin - ODU\ oxid$$

$$\phi(z) = \phi_\infty + (\phi_0 - \phi_\infty) \exp(-z/z_{por})$$

$$D_b(z) = D_b^0 \exp(\max(0, -(z - z_b)))$$

The rate of oxygen decrease is modelled accurately. Greenwood et al. (2010) calculated a decrease of 103 μM during the stratified period (end of April to beginning of September) over 138 days (average daily decrease of 0.75 $\mu\text{M d}^{-1}$). Our study indicates a decrease by 115 μM over the same period (corresponding to an average daily decrease of 0.83 $\mu\text{M d}^{-1}$). The oxygen concentration in the bottom water increases rapidly when the stratification is broken in autumn. The timing of the break-up of stratification is rather stochastic, and depends on the arrival of a sufficiently powerful autumn storm. After that, the oxygen concentration increases slowly further due to increased solubility with lower water temperatures in winter (Fig. 6).

While the model captures the overall oxygen decrease following the spring bloom rather well, there are some discrepancies between model output and data. As seen in Fig. 6, the CEFAS buoy data reveal a “bumpy” decrease of the bottom water oxygen, with strong upward and downward excursions, while the model simulates a more smooth and gradual decrease of the oxygen in the bottom water. The origin of these short and strong excursions is not clear, but resuspension events and internal waves have been suggested as possible causes (Greenwood et al., 2010). Such processes are not

accounted for in the present model formulation. The model also simulates an oxygen increase at depth when the phytoplankton blooms starts, which is not apparent in the data. This mismatch indicates that the onset of stratification is potentially not properly captured. This issue could not be resolved by calibrating the model. Ignoring a salinity effect on the stratification and the use of a one dimensional model (rather than a three dimensional model) are potential causes of this discrepancy.

Being a depocentre, sedimentary processes play an important role in the Oyster Grounds, particularly with respect to the oxygen consumption in the bottom layers and in the cycling of carbon and nitrogen (van der Molen, 2002; Osinga et al., 1996; Weston et al., 2008). For such areas the incorporation of a benthic biogeochemical submodel is necessary to arrive at a representative simulation of a shelf sea ecosystem (Middelburg and Levin, 2009; Soetaert and Middelburg, 2009). By incorporating a benthic compartment in the model, the importance of benthic processes in mineralization and oxygen demand can be assessed.

Our model simulation estimates the contribution of the sediment to the total organic matter degradation at 37% (averaged over the year 2007). Similar estimates have been

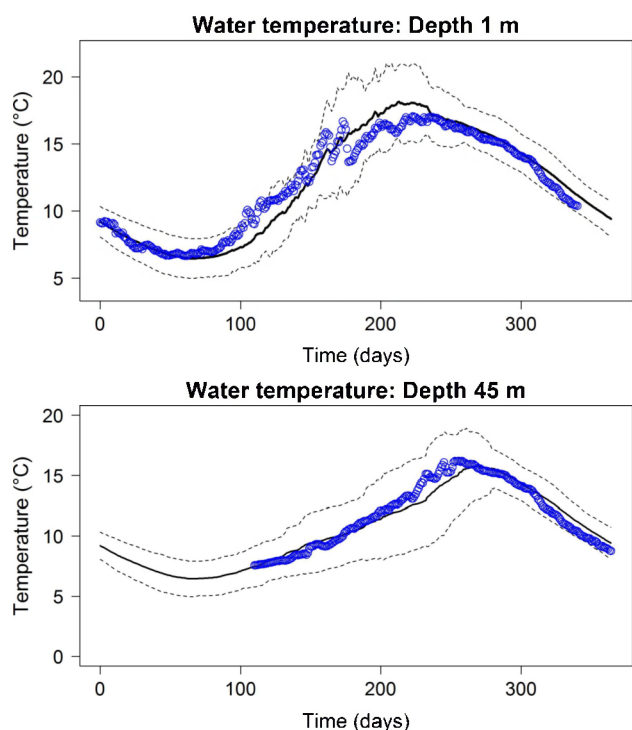


Fig. 4. Water temperatures at depths of 1 m and 45 m for the year 2007. The mean of 16 ensemble runs of the hydrodynamic model (black solid line), the 95 % confidence interval of these ensemble runs (black dashed line). The observational data from by the CEFAS buoy (blue points) are shown.

found by other modelling studies in shallow shelf seas with similar water depths (Heip et al., 1995; Middelburg and Soetaert, 2005; Soetaert and Middelburg, 2009). Field studies provide a range from 16 to 55 % in southern North Sea sediments (Upton et al., 1993), while Osinga et al. (1996) reported for the Oyster Grounds a high contribution of 79 to 119 %. The simulated organic matter mineralization rate in the sediment is $\sim 48 \text{ g C m}^{-2} \text{ yr}^{-1}$. This estimate lies well within the previous reported range for the Oyster Grounds of 41 to $46 \text{ g C m}^{-2} \text{ yr}^{-1}$ (De Wilde et al., 1984) but is again lower than the high mineralization value of $131 \text{ g C m}^{-2} \text{ yr}^{-1}$ reported by Osinga et al. (1996).

The processing of detrital organic matter in the sediment leads to an average benthic oxygen consumption rate of $8.6 \text{ mmol m}^{-2} \text{ d}^{-1}$. The sediment oxygen consumption varies, however, considerably over the year, strongly increasing in late spring due to an increased detritus supply to the bottom and increasing sediment temperature. The sediment oxygen consumption reaches its maximum at the end of September with an uptake rate of $17.5 \text{ mmol m}^{-2} \text{ d}^{-1}$, which is slightly higher than the values measured by Neubacher et al. (2011) ($9.1 \text{ mmol O}_2 \text{ m}^{-2} \text{ d}^{-1}$ in September 2007 and $15.1 \text{ mmol O}_2 \text{ m}^{-2} \text{ d}^{-1}$ in October 2007). Uptake rates measured at the end of September by Weston et al. (2008) were on average higher ($24 \text{ mmol O}_2 \text{ m}^{-2} \text{ d}^{-1}$), but our simulated

oxygen flux lies within the range observed between the different stations sampled by these authors (ranging from 12.5 to $30 \text{ mmol O}_2 \text{ m}^{-2} \text{ d}^{-1}$). The values reported by Osinga et al. (1996) again show higher values for the oxygen uptake (yearly average of $35 \text{ mmol O}_2 \text{ m}^{-2} \text{ d}^{-1}$).

The importance of mineralization in the sediment is also reflected in high fluxes of nitrate and ammonium across the sediment–water interface following the spring bloom (Rauch and Denis, 2008). On average the flux of nitrate and ammonium is $0.5 \text{ mmol m}^{-2} \text{ d}^{-1}$ and $0.3 \text{ mmol m}^{-2} \text{ d}^{-1}$, respectively. These values are comparable with fluxes measured by Neubacher et al. (2011) and Weston et al. (2008). During stratification, the flux of nitrate and ammonium from the sediment leads to the accumulation of these nutrients in the bottom water as stratification blocks any further upward transport (Soetaert and Middelburg, 2009, Fig. 6). When the stratification is broken, the nutrients are homogenized in the water column. In winter they increase to a maximum concentration due to continued mineralization, occurring mainly in the sediment, while there is almost no uptake by phytoplankton.

3.3 Future situation in the Oyster Grounds

Upon comparison with the available observational data and with information from the literature, the simulations of the calibrated model over the year 2007 seem to adequately capture the main biogeochemical processes affecting carbon, nitrogen and oxygen cycling in the Oyster Grounds. In a next step we combined this model parameterization with the atmospheric forcings over 2000–2100 predicted by the ESSENCE climate model to make projections on the future evolution of the oxygen dynamics within the Oyster Grounds. The aim was to quantify how the bottom water oxygen concentration in the Oyster Grounds evolves with global change (Greenwood et al., 2010; Weston et al., 2008) and to clarify the role of the different drivers on the evolution of hypoxia.

Future projections are always subject to simplifying assumptions since it is plainly impossible to take all effects of global change into account in the model setup. Therefore, this study focuses on the effect of changing climate forcings (mainly the effect of air temperature and wind) and the effect of changing nutrient loadings. This implies that other effects of global change, like changes in circulation patterns resulting from climate change or salinity changes due to an intensified hydrological cycle, are not incorporated. Since currents play a strong role in oxygen transport, oxygen dynamics could be strongly affected by changes in circulation. Three-dimensional (3-D) hydrodynamic model simulations for the larger North Sea area are essential in order to be able to predict the impact of changing currents. However, it should be noted that such 3-D models pose additional challenges in terms of boundary conditions and parameterization, which introduce additional uncertainties in simulations over the next 100 yr.

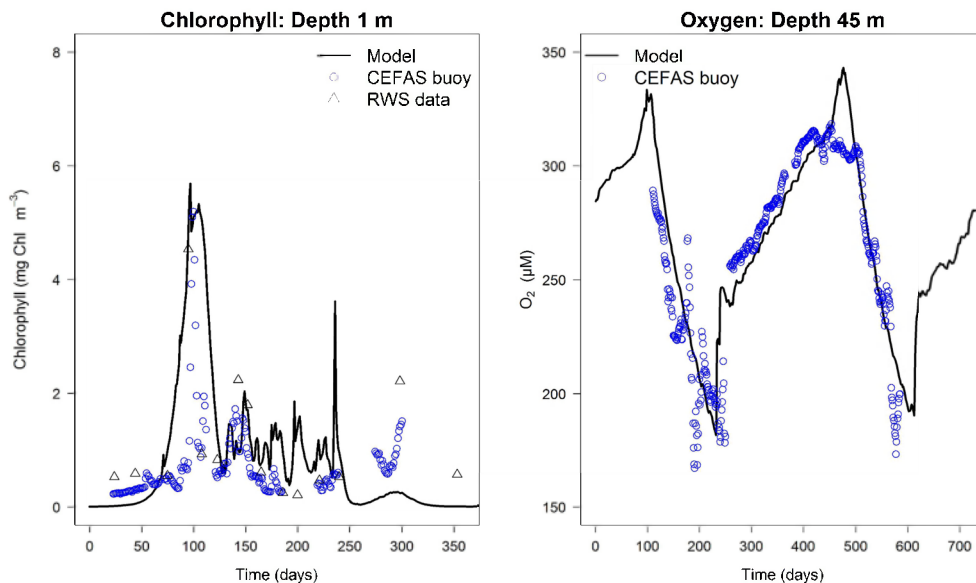


Fig. 5. The left panel shows a comparison between chlorophyll concentration calculated by the coupled benthic–pelagic model (black solid line) and the concentration measured by the CEFAS buoy (blue points) and Rijkswaterstaat (RWS) monthly monitoring data (black triangles) for a simulation of the year 2007. The right panel shows the calibration result of the oxygen concentration at a depth of 45 m for the period 2007–2008.

3.3.1 Future climatic forcings

A comparison of the ESSENCE simulations for the period 2000–2010 versus 2090–2100 shows a strong increase of the air temperature – on average 2.3°C (Fig. 7) (Sterl et al., 2009). There are, however, strong seasonal differences: warming is most pronounced in the winter months with an average warming in February and March of 2.7° , while it is only 2.1°C in summer (Fig. 7). Other climate simulations for the North Sea predict a similar seasonal pattern in temperature increase by 2100 (Giorgi et al., 2004; Lowe et al., 2009). Note that these temperature changes are principally determined by the selection of the SRES A1B greenhouse emission scenario that underlies the ESSENCE simulations (Sterl et al., 2009).

In contrast to temperature, climate models show less consensus on how wind conditions in the North Sea area will be affected by climate change. In fact, the ESSENCE simulations predict no appreciable changes in wind speed and direction. Both the periodicity and magnitude of wind is comparable between 2000–2010 and 2090–2100 (Fig. 7). Statistical analysis of the wind simulations showed only a small increase in the strong southwesterly winds for the region from 53°N to 55°N . The detected differences were smaller than the natural variability and therefore statistically insignificant (Sterl et al., 2009). Also, the storm intensity or frequency (defined as events with wind speed in excess of 24.5 m s^{-1}) does not change significantly for the period 2000–2010 compared with the period 2090–2100 (Sterl et al., 2009). Young et al. (2011) predict also no changes for the North Sea, and

Woth et al. (2005) found only a very small increase of up to 1 m s^{-1} for the 99th percentile of the wind speed. Stronger increases in extreme wind speed of 5% and 10% have been found by Räisänen et al. (2004) and the STOWASUS-2100 group (Beniston et al., 2007; Kaas and Group, 2001), respectively. But the pattern of the changes and the exact increase depends strongly on the particular model used and the applied emission scenario.

3.3.2 Effect of changing climate forcings (at constant nutrient loadings)

The physical model projects an increase of the future surface water temperature in the Oyster Grounds by $\sim 2.1^{\circ}\text{C}$. This lies within the range projected by Lowe et al. (2009), but is higher than the average increase by 1.7°C in the North Sea reported by Ådlandsvik (2008), who used the SRES A1B scenario for the period 2072–2097 in a downscaled Bergen Climate Model (BCM) to model the marine climate in the North Sea.

Next to a strong increase in the water temperature, our simulations predict an enhanced stratification (Fig. 8). In the period 2000–2010, stratification starts in early spring, beginning of April and is disrupted at the end of September. By 2090–2100, stratification becomes stronger, both in duration as well as in intensity. Although stratification does not start earlier, it lasts longer – until October. On average the stratification period increases by 10 days (Fig. 8), which results in an additional decrease of $7.5\text{ }\mu\text{M}$ in bottom oxygen concentration, assuming a decrease rate of $0.75\text{ }\mu\text{M d}^{-1}$. Lowe

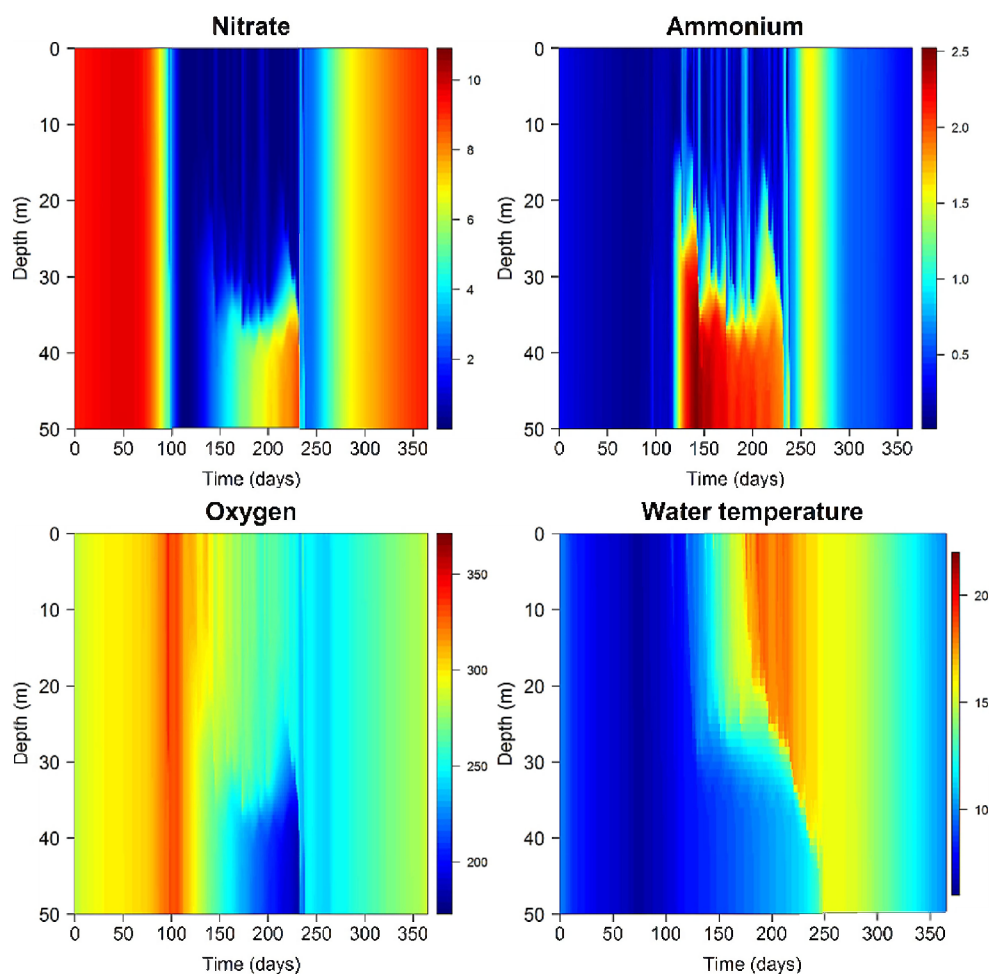


Fig. 6. Spatio-temporal plots of the nitrate, ammonium, oxygen concentrations (in mmol m^{-3}) and temperature ($^{\circ}\text{C}$) for the year 2007.

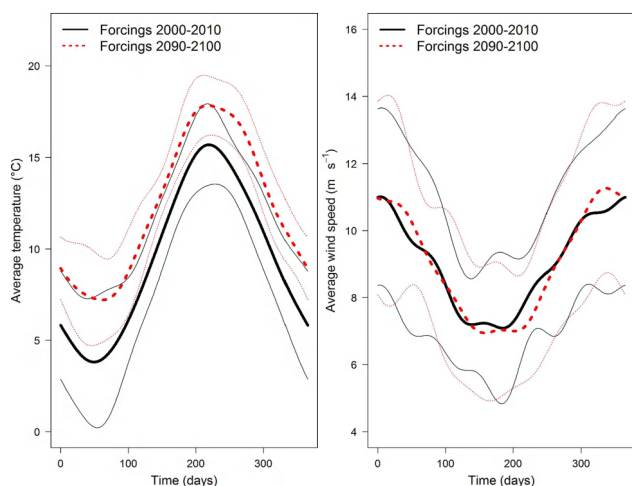


Fig. 7. Comparison between present climate forcings (2000–2010) (black solid line) and future climate forcings (2090–2100) (red dotted line) for air temperature (left) and wind speed (right). The daily averaged value of the 16 different climate simulations for a period of 10 yr is plotted together with the 95% confidence interval.

et al. (2009) report a similar delay of the stratification breakdown, but they also predict an earlier onset of the stratification by 10 days (which then would lead to a decrease of $15 \mu\text{M}$ in bottom oxygen concentration).

Our model simulations also predict an increase in the intensity of stratification, as quantified by the maximum difference in temperature between cold bottom water and warm surface water. Generally, this stratification intensity parameter increases by 0.5°C between present day and the end of the 21st century (Fig. 8). A similar intensification of stratification due to warmer surface water temperatures is also predicted by other studies (Conley et al., 2009; Keeling et al., 2010; Peña et al., 2010; Rabalais et al., 2010). Since no significant changes in storm events are projected for the ESSENCE climate forcings, our model does not predict any wind-induced effects on stratification for the Oyster Grounds.

The output of the biogeochemical model shows marked differences under future climate forcings when compared to present-day conditions. The phytoplankton bloom occurs on

Table 8. Parameter values of the pelagic ecosystem model. All rate parameters are defined at 20 °C.

Symbol	Value	Quantity	Unit	Reference
k_w	0.198	Extinction coefficient water	m^{-1}	Lund-Hansen (2004)
k_p	0.029	Extinction coefficient phytoplankton	$m^{-1} (mmol\ m^{-3})^{-1}$	Lund-Hansen (2004)
Q_{10}	2	Temperature dependence metabolic rates	–	Soetaert et al. (2001)
T_{ref}	20	Reference temperature metabolic rates	°C	Soetaert et al. (2001)
Phytoplankton				
I_{opt}	20	Optimum light intensity	$W\ m^{-2}$	Calibrated
μ_{max}	1.8	Maximum growth rate	d^{-1}	Soetaert et al. (2001)
K_{NH_4}	0.3	Half-saturation concentration for NH_4 uptake	$mmol\ m^{-3}$	Soetaert et al. (2001)
K_{NO_3}	0.5	Half-saturation concentration for NO_3 uptake	$mmol\ m^{-3}$	Oguz et al. (1999)
ψ	1.5	Inhibition coefficient for NH_4	$mmol\ m^{-3}$	Chapelle et al. (2000)
m_{PHYTO}	0.02	Mortality rate constant	d^{-1}	Calibrated
w_{PHYTO}	0.2	Sinking speed phytoplankton	$m\ d^{-1}$	Soetaert et al. (2001)
Zooplankton				
g_{max}	0.8	Maximum grazing rate	d^{-1}	Calibrated
K_{PHYTO}	0.6	Half-saturation concentration grazing	$mmol\ m^{-3}$	Denman et al. (1998)
q_{ZOO}	0.7	Growth efficiency	–	Schrum et al. (2006)
m_{ZOO}	0.25	Mortality rate constant	$d^{-1} (mmol\ m^{-3})^{-1}$	Calibrated
r_{ZOO}	0.08	Excretion and respiration rate zooplankton	d^{-1}	Calibrated
Biogeochemistry				
r_{min}	0.05	Mineralisation rate constant	d^{-1}	Lee et al. (2002)
r_{ODU}	1	ODU oxidation rate constant	d^{-1}	Cline and Richards (1969)
r_{nit}	0.1	Nitrification rate constant	d^{-1}	Lee et al. (2002)
K_{O_2}	3	Half-saturation concentration for O_2 limitation	$mmol\ m^{-3}$	Soetaert et al. (2001)
w_{DET}	1	Sinking speed detritus	$m\ d^{-1}$	Soetaert et al. (2001)
Stoichiometry				
γ_{OC}^N	6.625	C : N ratio; Redfield Ratio	$mol\ C\ mol\ N^{-1}$	
$\gamma_{O_2}^{NH_4}$	6.625	Mol O_2 produced per mol NH_4 uptake	$mol\ O_2\ mol\ NH_4^{-1}$	
$\gamma_{O_2}^{NO_3}$	8.625	Mol O_2 produced per mol NO_3 uptake	$mol\ O_2\ mol\ NO_3^{-1}$	
$\gamma_{O_2}^C$	1	Mol O_2 consumed per mol C mineralized	$mol\ O_2\ mol\ C^{-1}$	

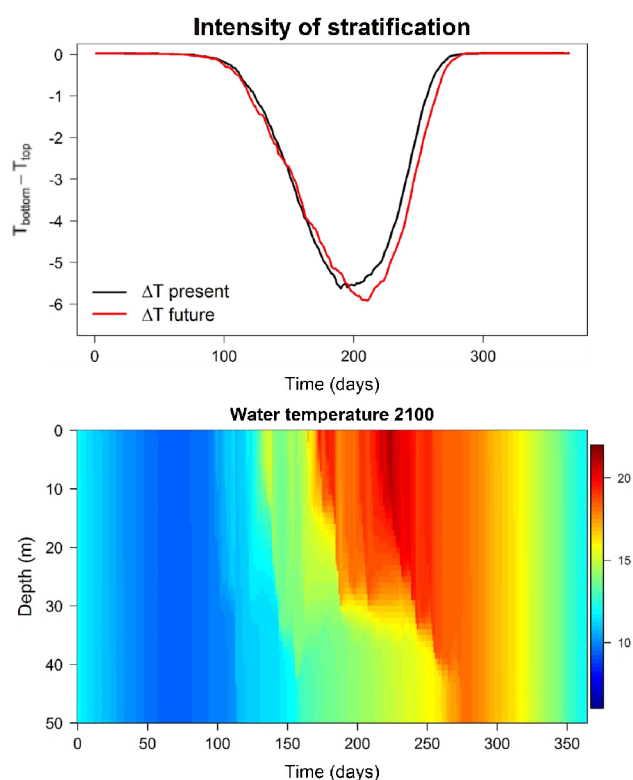
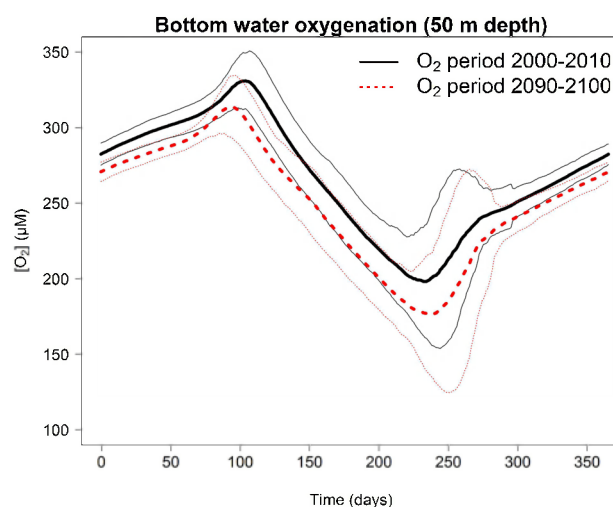
average ten days earlier and primary production increases by 11 %. Faster cycling of the nutrients in the surface mixed layer leads however to a decrease of the relative contribution of benthic mineralization to the total mineralization, diminishing from 37 % to 33 %. Figure 9 compares the bottom water oxygen concentration for the period 2000–2010 and the period 2090–2100. Averaged over the whole year, the oxygen concentration at 50 m depth (bottom layers) is 17 μM (6.5 %) lower for the period 2090–2100 compared with the period 2000–2010. The difference between the oxygen concentration in the bottom layer under present and future climate forcings shows, however, a strong interannual variability. Figure 10 shows the percentage decrease of the oxygen concentration in the bottom layer under future climate forcings compared with present climate forcings. In winter the decrease is smallest ($\sim 5\%$ or 13 μM), but the difference increases during the late summer (day 230–270) to 24 μM or $\sim 11.5\%$.

The decrease in the oxygen concentration can be attributed to different factors. First of all, temperature plays a crucial

role in controlling the extent of hypoxia (Conley et al., 2009; Keeling et al., 2010). Higher water temperature reduces the solubility of oxygen, leading to a loss of dissolved oxygen or “deoxygenation”. On a global scale, ocean models predict a decline of the global ocean O_2 inventory with 1 to 7 % over the next century (Keeling et al., 2010). To calculate what the effect of reduced oxygen solubility at higher water temperature is, the oxygen solubility in the present bottom water is compared with future conditions. For the Oyster Grounds, a 2.1 °C warmer bottom layer will lead to an average loss of dissolved oxygen by 12.2 μM ($\sim 5\%$) (Fig. 10) (Weston et al., 2008). On a yearly basis this implies that the reduced oxygen solubility is responsible for 65 % of the oxygen decrease in the future. The solubility effect explains the future decrease of O_2 during winter months, but not during summer. At the end of the summer (day 230–270) other mechanisms clearly play a role: the oxygen decrease in that period is more pronounced than expected from the solubility effect alone (Fig. 10). During this period the solubility is only responsible for 27 %.

Table 9. Parameter values of the benthic ecosystem model. All rate parameters are defined at 0 °C.

Symbol	Value	Quantity	Unit	Reference
Q_{10}	2	Temperature dependence metabolic rates	–	Soetaert et al. (2001)
r_{fast}	0.01	Mineralization rate of the most reactive organic C fraction	d^{-1}	Soetaert et al. (1996a)
r_{slow}	0.00001	Mineralization rate of the least reactive organic C fraction	d^{-1}	Soetaert et al. (1996a)
p_{Fast}	0.9	Fraction of most reactive detritus fraction in flux	–	Assumed
r_{nit}	20	Maximum nitrification rate	d^{-1}	Soetaert et al. (1996b)
r_{ODU}	20	Maximum oxidation rate of ODU	d^{-1}	Soetaert et al. (1996b)
K_{SO_2}	3	Half-saturation conc for O_2 limitation in oxic mineralization	mmol m^{-3}	Soetaert et al. (1996b)
K_{NO_3}	30	Half-saturation conc for NO_3 limitation in denitrification	mmol m^{-3}	Soetaert et al. (1996b)
$K_{\text{in}}^{\text{Denit}}$	10	Half-saturation conc for O_2 inhibition in denitrification	mmol m^{-3}	Soetaert et al. (1996b)
$K_{\text{in}}^{\text{Anoxmin}}$	1	Half-saturation conc for O_2 inhibition in anoxic mineralization	mmol m^{-3}	Soetaert et al. (1996b)
$K_{\text{in}}^{\text{Anoxmin}}_{\text{NO}_3}$	1	Half-saturation conc for NO_3 inhibition in anoxic mineralization	mmol m^{-3}	Soetaert et al. (1996b)
NH_4^{ads}	1.3	Adsorption coefficient of ammonium	–	Soetaert et al. (1996b)
$\gamma_{\text{OC}}^{\text{N}}$	6.625	C:N ratio; Redfield Ratio	mol C mol N^{-1}	Soetaert et al. (1996b)
D_{b}^0	10	Bioturbation coefficient in the bioturbated layer	$\text{cm}^2 \text{yr}^{-1}$	Assumed
z_{b}	5	Depth below which the bioturbation decreases exponentially	cm	Assumed
ϕ_0	0.7	Porosity at the sediment–water interface	–	Assumed
ϕ_{∞}	0.5	Porosity at infinite sediment depth	–	Neubacher et al. (2011)
z_{por}	2	Attenuation depth porosity	cm	Assumed

**Fig. 8.** Intensity of the stratification calculated as the difference between the water temperature in the bottom and the top layer for present (2007) and future (2100) water column (top panel). The bottom panel shows the water temperature for the year 2100 as calculated by the physical model.**Fig. 9.** Evolution of the yearly oxygen concentration for the period 2000–2010 (black solid line) and period 2009–2100 (red dotted line) at the bottom layer of the Oyster Grounds. The curves are the average value of the 16 simulations for each period. The 95 % confidence interval is also indicated.

A second factor that influences the oxygen concentration in the water is the effect of increased temperature on the biological processes. To assess to which extent the direct control of temperature on biological process rates is important (higher process rates due to Q_{10} factor), we neutralized the effect of the average water temperature increase by 2.1 °C on biological processes. This is done by shifting the temperature optimum of all biological processes by 2.1 °C (Fig. 10). Due

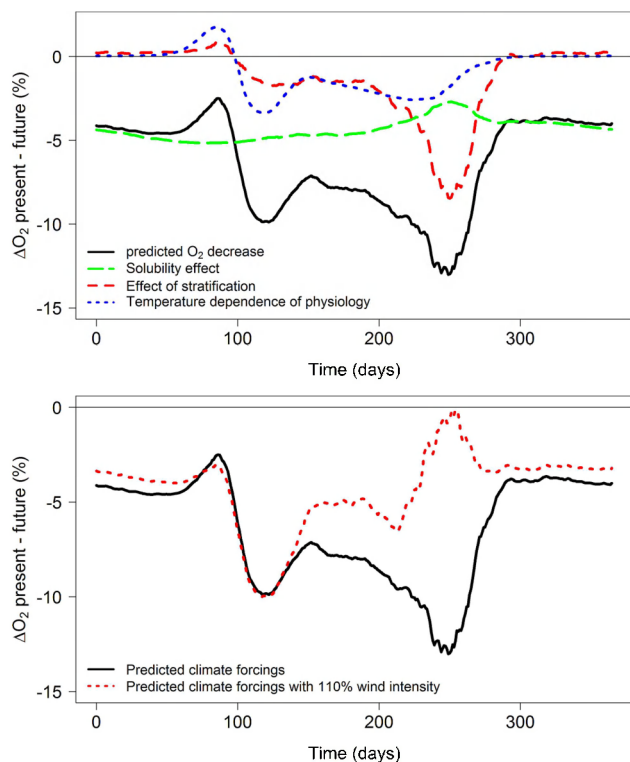


Fig. 10. Top panel shows predicted percentage decrease of oxygen concentration at 50 m depth between present (period 2000–2010) and future (period 2090–2100), partitioned amongst different factors: solubility, physical factors (stratification) and the effect of temperature dependence on the physiology. The curves show the average of 16 simulations. Bottom panel shows a comparison between the decrease in oxygen concentration at 50 m depth using the projected future forcings and future forcings with 110 % wind intensity.

to the earlier spring bloom under future climate forcings, a clear effect in early spring can be seen. On average, the phytoplankton blooms ten days earlier due to warmer water temperatures. This shifts the period of oxygen oversaturation of the water column due to photosynthesis. Also, a faster cycling of the nutrients in the upper layers lowers the relative importance of the benthic system (by $\sim 5\%$), but due to the higher NPP, the absolute rate of mineralization in the deeper layers increases (Conley et al., 2009). Overall, the temperature dependence of biogeochemical cycling has only a relatively minor effect of 13 % on the observed oxygen decrease on an annual basis. This increases slightly to 15 % during the end of the summer.

A final aspect that strongly influences the oxygen concentration is water column stratification since it controls the supply of oxygen to the bottom layers (Conley et al., 2009; Keeling et al., 2010; Peña et al., 2010; Rabalais et al., 2010). Future enhancement of stratification is expected to lead to longer and stronger depletion of oxygen in the bottom layers (Justic et al., 1996). This is also seen in the current model simulations. The effect of stratification (and potentially other

physical drivers) on the bottom water oxygen concentration was calculated by subtracting the biological and solubility effect from the projected overall decrease. The strong oxygen decrease observed at the end of summer (Fig. 10) coincides with the observed strengthening of stratification (Fig. 8a). Overall, our model simulations predict that enhanced stratification will decrease the bottom water oxygen concentration by 22 % at the end of the 21st century. But during the end of the summer, the period of lowest bottom oxygen concentrations, the importance of stratification increases to 58 %. This indicates that on an annual basis, the solubility effect is more important than the effect of enhanced stratification. But during the summer months, stratification clearly has a much stronger effect on the bottom oxygen concentrations, being around twice as important as the solubility effect. Since stratification mostly occurs when biological oxygen consumption is maximal, stratification is obviously a crucial factor in oxygen depletion in bottom layers. Also, Keeling et al. (2010) indicated that enhanced stratification has a strong effect (2 to 4 times stronger than the effect of the solubility).

3.3.3 Effect of increased wind speed and storm frequencies

The ESSENCE simulations predict hardly any changes in the wind speed over the central North Sea between the periods 2000–2010 and 2090–2100 (Fig. 7). As a result, the ESSENCE climate forcings does not show any impact of wind changes on the prevalence of future hypoxia. Other climate model simulations, however, indicate that wind patterns might change in the North Sea, and predict an increase of up to 10 % in the extreme wind speeds at the end of the 21st century (Kaas and Group, 2001; Rauthe and Paeth, 2004; Rockel and Woth, 2007). To investigate the effect of wind speed on hypoxia development, the wind speed was increased with 10 % in the 2090–2100 climate forcings resulting from the ESSENCE simulations. Note that this flat increase of the wind speed (i.e. 10 % across the spectrum) is a simplifying assumption, and presumably too strong in comparison to the projected changes in the wind speed (Kaas and Group, 2001; Woth et al., 2005).

Increasing the wind speed has a substantial effect on the future oxygen concentrations in the bottom waters at the Oyster Grounds (Fig. 10). In the winter period the results are similar with and without artificial wind increase. The predicted decrease of $\sim 4\%$ in the winter bottom water O_2 levels over 2090–2100 can be completely attributed to the decreased solubility of oxygen with increasing water temperature (Fig. 10a). Additional wind-induced turbulence does not affect the oxygen level in the bottom waters in winter times since the water column is already fully mixed. In the summer period, however, the increased wind speed results in a more frequent ventilation of the bottom water, and hence it decreases the risk of strong oxygen depletion in the bottom layers. This wind-induced mixing strongly counteracts the

stronger stratification (Fig. 10b). The effect is especially noticeable in late summer and early autumn, when normally the lowest bottom oxygen concentrations occur. The increased prevalence of strong winds disrupts the stratification earlier (\sim after 150 days instead of 250 days), thus enhancing ventilation of the bottom layer and reducing the period of lowered oxygen concentrations in the bottom water.

The bottom water O_2 levels are still lower when compared to the present situation due to the interplay of reduced solubility and higher respiration rates (Fig. 10a).

3.4 Effect of changing nutrient loadings

The simulations as discussed up to now include only the effect of changes in climatological conditions on the bottom water oxygen concentrations. However, coastal zones are also affected by changes in nutrient delivery from land, which is another important component of global change. The input of nutrients to coastal ecosystems has recently accelerated due to various human activities (Diaz and Rosenberg, 2008). An increased nutrient loading enhances the primary production in the coastal zone, which then leads to higher flux of organic material to the bottom layers causing oxygen depletion in the deeper layers (Conley et al., 2009). The strong relation between nutrient loadings and the intensity and extent of hypoxia has been shown by models and observations (Middelburg and Levin, 2009; Rabalais et al., 2002; Soetaert and Middelburg, 2009). However, an open question is how the effect of nutrient forcings on hypoxia quantitatively compares to the effect of climate forcings. To investigate this for the Oyster Grounds, our coupled physical–biogeochemical model was run with different nutrient forcings using the present climate forcings (ensemble of 16 ESSENCE meteo forcings for the year 2000), and subsequently the same exercise was repeated for the future climate forcings (ensemble of 16 ESSENCE meteo forcings for the year 2100).

3.4.1 Effect of changing nutrient loadings using present climate forcings

As discussed above, the nutrient forcing of the model is determined by the total nitrogen pool in winter conditions that is initially imposed upon the model (any loss of N from denitrification is directly compensated for, keeping the total N pool constant). Monthly monitoring data of Rijkswaterstaat indicate a mean concentration of total dissolved nitrogen (TDN) in winter of 11 mmol N m^{-3} over the period 2000–2010, but varying from 6 to 20 mmol N m^{-3} between different years (Waterbase, Rijkswaterstaat). This high inter-annual variability in the TDN concentration can be explained by changes in the sources of the water masses at the Oyster Grounds and associated differences in nutrient input (Skogen and Moll, 2000; Vermaat et al., 2008). For the Oyster Grounds, the Atlantic and Channel water masses contribute

on average 70 % to the nutrient concentration, while the remaining 30 % of the nitrogen can be attributed to riverine inputs, mainly from the Humber. Using various transport models, the anthropogenic contribution to the total nitrogen concentration within the Oyster Ground area has been estimated at 25 % (OSPAR, 2007).

We performed simulations where TDN ranged from 6 to 20 mmol N m^{-3} to capture the current year-to-year variability in winter concentrations in the Oyster Grounds. Over this range of nutrient loadings, the yearly averaged primary production increases from $8 \text{ mol C m}^{-2} \text{ yr}^{-1}$ ($95 \text{ g C m}^{-2} \text{ yr}^{-1}$) to $24 \text{ mol C m}^{-2} \text{ yr}^{-1}$ ($290 \text{ g C m}^{-2} \text{ yr}^{-1}$). This increased primary production also leads to an associated increase in the flux of organic matter to the bottom water and sediment (ranging from 30 to $85 \text{ g C m}^{-2} \text{ yr}^{-1}$).

This higher export results in a higher oxygen demand in the bottom water causing stronger oxygen depletion, as expressed by the minimum O_2 concentration reached in the bottom waters. The minimum oxygen concentration at a given nutrient forcing depends strongly on the meteorological forcings, as shown by the strong differences between the 16 different simulations for the year 2000 (Fig. 11: upper panel). The interplay of year-to-year variability in the nutrient loadings with year-to-year variability in the meteo forcings allows that the realized minimum oxygen concentration in the bottom layer can vary significantly between subsequent years. The realized state in one year must lie within the rectangular “window of oxygen depletion” as drawn in Fig. 11 (upper panel), with associated bottom water oxygen concentrations ranging from 100 to $210 \mu\text{M}$. This oxygen depletion window provides an explanation for the strong year-to-year variability observed in the bottom water oxygen concentrations ($65\text{--}203 \mu\text{M}$) (Greenwood et al., 2010; Queste et al., 2012; Weston et al., 2008). This oxygen depletion window can also be used to assess the risk of hypoxia in the Oyster Grounds. Under present climate forcings, the oxygen depletion window lies entirely above the horizontal line of the hypoxia threshold, and so our model simulations do not predict the occurrence of hypoxia in the Oyster Grounds. When the highest pelagic nitrogen concentration and extreme climate forcings are combined, the oxygen drops as low as $100 \mu\text{M}$. This low oxygen concentration is slightly higher than the lowest oxygen concentration in the Oyster Grounds yet observed, which was recorded in the warm summer of 2003 (Weston et al., 2008).

3.4.2 Effect of changing nutrient loadings using future climate forcings

The risk of hypoxia is expected to increase with climate change. Some authors have argued that high nutrient loadings will have a much more pronounced effect on the oxygen concentrations under future climate forcings (Justić et al., 2005; Rabalais et al., 2009). Our simulation results fully support this argument. Assuming that the pelagic nitrogen

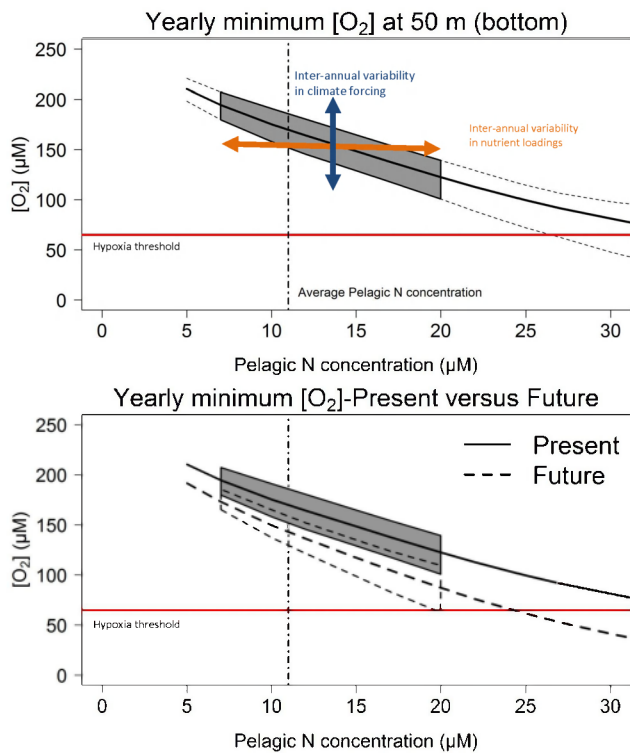


Fig. 11. Effect of increasing pelagic nitrogen concentration on the yearly minimum oxygen concentration ($[O_2]$) at 50 m depth (bottom). The current average pelagic nitrogen concentration ($11 \mu\text{M}$) is indicated with a vertical dashed line. The horizontal red line at $63 \mu\text{M}$ indicates the hypoxia threshold. Top panel: using present climate forcings (year 2000). The dotted lines indicate the minimum and maximum concentration of the different climate simulations of 2000; polygon indicates the likely area of oxygen concentrations. The arrows indicate the interannual variability in climate forcings and nutrient loadings. Bottom panel: comparison between present (year 2000) and future climate forcings (year 2100). The polygon is grey for the present climate forcings and transparent (dotted line) for the future climate forcings.

concentration in 2090–2100 will vary within the same range as in the period 2000–2010, a similar oxygen depletion window can be drawn, taking into account the variability due to nutrient loadings and climate forcings. Under future climate forcings, the oxygen depletion window is shifted downward and drops partly below the hypoxia threshold line (Fig. 11, bottom panel). Hence, under future climate forcings, the risk for potential hypoxia in the Oyster Grounds clearly increases. In particular, our model simulations show that the bottom water oxygen concentration in the Oyster Grounds can pass the hypoxia threshold under specific meteorological forcings in 2090–2100 (i.e. long, warm summers), and can drop as low as $60 \mu\text{M}$. These results stress the importance of an efficient nutrient control management in the future (Fig. 12). Only under lower nutrient loadings can the increased risk of hypoxic conditions due to changing climate forcings be countered.

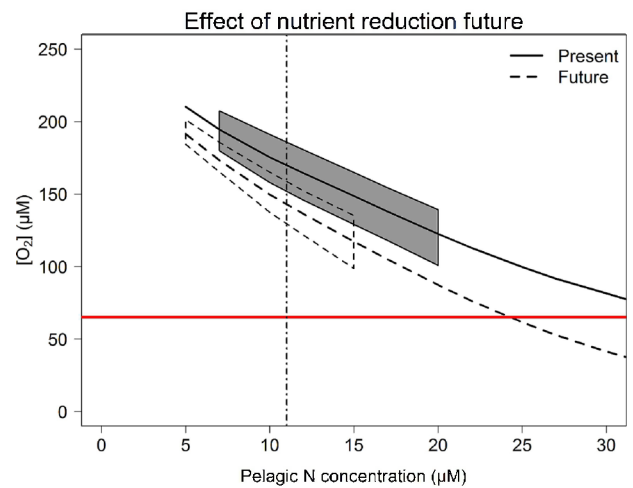


Fig. 12. Relation between pelagic nitrogen concentration and the yearly minimum oxygen concentration ($[O_2]$) at 50 m depth (bottom) for present and future climate forcings. The present average pelagic nitrogen concentration ($11 \mu\text{M}$) is indicated with a vertical dashed line. The horizontal red line at $63 \mu\text{M}$ indicates the hypoxia threshold. The polygon indicates the likely area of oxygen concentrations. The polygon is grey for the present climate forcings and transparent (dotted) for the future climate forcings with nutrient reduction.

We need a reduction in the maximum total dissolved nitrogen concentration of about $5 \mu\text{M}$ over 100 yr to maintain the Oyster Grounds at the current risk level of hypoxia. Therefore, a more rigid control of the nutrient loadings in coastal systems is essential. Efforts to decrease nutrient loadings in coastal shelf seas will pay off by decreasing the susceptibility of these stratified shelf seas to turn periodically hypoxic.

4 Summary and conclusion

Changes in both climate forcings and nutrient runoff associated with global change will have a strong impact on stratified coastal ecosystems. To assess the role of these different drivers on the evolution of the bottom water oxygen concentrations, a one-dimensional ecosystem model was developed, which was calibrated for the Oyster Grounds, an area that periodically experience lower bottom O_2 concentrations. Our results indicate that the projected changes in climatological conditions for the North Sea over the next 100 yr will increase the risk of hypoxia in the Oyster Grounds. The yearly minimum bottom water oxygen concentration is predicted to decrease on average by $17 \mu\text{M}$ by 2100, but during the end of the summer a stronger decrease of $24 \mu\text{M}$ is expected. Based on our model simulations, the decrease during the end of the summer could be attributed to a reduced solubility of oxygen at higher water temperature (27%), a reduced transport of O_2 to bottom layers due to enhanced stratification (58%) and increased biological oxygen demand (15%). Nutrient loadings

also strongly impact the risk of hypoxia. Higher nitrogen concentration leads to lower bottom oxygen concentration and an increased risk of hypoxia. These findings confirm that nutrient loadings are a strong driver for hypoxia (Rabalais et al., 2002). Keeping the nutrient levels at current conditions, the Oyster Grounds consequently might periodically become hypoxic by the year 2100. Therefore, continued eutrophication management will be essential to avert the potential development of low oxygen concentration in the Oyster Grounds.

Acknowledgements. The research leading to these results has received funding from the European Union's Seventh Framework Programme HYPOX under grant agreement no. 226213. This research was further supported by the Research Foundation – Flanders (FWO Odysseus grant to FJRM and FWO aspirant grant to LM) and the Netherlands Organization for Scientific Research (VIDI grant to FJRM). This publication contributes to the Darwin Institute for Biogeosciences. We thank Naomi Greenwood (CEFAS) for providing access to the SmartBuoy dataset and Remi Laane for providing the RWS monitoring data of the Oyster Grounds. We thank Andreas Sterl for generously providing access to the climate simulation output of the ESSENCE project, and Piet Ruardij for the data that enabled calibration of the hydrodynamic model.

Edited by: B. Dewitte

References

- Ådlandsvik, B.: Marine downscaling of a future climate scenario for the North Sea, *Tellus A*, 60, 451–458, doi:10.1111/j.1600-0870.2008.00311.x, 2008.
- Beniston, M., Stephenson, D. B., Christensen, O. B., Ferro, C. A. T., Frei, C., Goyette, S., Halsnæs, K., Holt, T., Jylhä, K., Koffi, B., Plutikof, J., Schöll, R., Semmler, T., and Woth, K.: Future extreme events in European climate: an exploration of regional climate model projections, *Climatic Change*, 81, 71–95, doi:10.1007/s10584-006-9226-z, 2007.
- Birchough, S. N. R., Parker, R. E., McManus, E., and Barry, J.: Combining bioturbation and redox metrics: potential tools for assessing seabed function, *Ecol. Indic.*, 12, 8–16, doi:10.1016/j.ecolind.2011.03.015, 2012.
- Boers, M.: Effects of a Deep Sand Extraction Pit, Final Report of the PUTMOR Measurements at the Lowered Dump Site, Rijksinstituut voor Kust en Zee/RIKZ, RIKZ/2005.001, The Hague, the Netherlands, ISBN 90-369-3498-2, 87 pp., 2005.
- Boon, A. R., Duineveld, G. C. A., and Kok, A.: Benthic organic matter supply and metabolism at depositional and non-depositional areas in the North Sea, *Estuar. Coast. Shelf S.*, 49, 747–761, doi:10.1006/ecss.1999.0555, 1999.
- Chapelle, A., Ménesguen, A., Deslous-paoli, J., and Souchu, P.: Modelling nitrogen, primary production and oxygen in a Mediterranean lagoon, impact of oysters farming and inputs from the watershed, *Ecol. Model.*, 127, 161–181, 2000.
- Cline, J. D. and Richards, F. A.: Oxygenation of hydrogen sulfide in seawater at constant salinity, temperature, and pH, *Environ. Sci. Technol.*, 3, 838–843, 1969.
- Conley, D. J., Carstensen, J., Vaquer-Sunyer, R., and Duarte, C. M.: Ecosystem thresholds with hypoxia, *Hydrobiologia*, 629, 21–29, doi:10.1007/s10750-009-9764-2, 2009.
- De Wilde, P. A. W. J., Berghuis, E. M., and Kok, A.: Structure and energy demand of the benthic community of the oyster ground, Central North Sea, *Neth. J. Sea Res.*, 18, 143–159, doi:10.1016/0077-7579(84)90029-2, 1984.
- Denman, K. L., Peña, M. A., and Haigh, S. P.: Simulations of Marine Ecosystem Response to Climate Variation with a One Dimensional Coupled Ecosystem/Mixed Layer Model Biotic Impacts of Extratropical Climate Variability in the Pacific Simulations of Marine Ecosystem Response to Climate Variation with, 141–147, 1998.
- Diaz, R. J.: Overview of hypoxia around the world, *J. Environ. Qual.*, 30, 275–81, available at: <http://www.ncbi.nlm.nih.gov/pubmed/11285887>, 2001.
- Diaz, R. J. and Rosenberg, R.: Spreading dead zones and consequences for marine ecosystems, *Science*, 321, 926–929, doi:10.1126/science.1156401, 2008.
- Gaspar, P., Grégoris, Y., and Lefevre, J.-M.: A simple eddy kinetic energy model for simulations of the oceanic vertical mixing: tests at station Papa and long-term upper ocean study site, *J. Geophys. Res.*, 95, 16179–16193, doi:10.1029/JC095iC09p16179, 1990.
- Gieskes, W. W. C. and Kraay, G. W.: Phytoplankton, its pigments, and primary production at a Central North Sea station in May, July and September 1981, *Neth. J. Sea Res.*, 18, 51–70, 1984.
- Giorgi, F., Bi, X., and Pal, J.: Mean, interannual variability and trends in a regional climate change experiment over Europe. II: Climate change scenarios (2071–2100), *Clim. Dynam.*, 23, 839–858, doi:10.1007/s00382-004-0467-0, 2004.
- Greenwood, N., Parker, E. R., Fernand, L., Sivyer, D. B., Weston, K., Painting, S. J., Kröger, S., Forster, R. M., Lees, H. E., Mills, D. K., and Laane, R. W. P. M.: Detection of low bottom water oxygen concentrations in the North Sea; implications for monitoring and assessment of ecosystem health, *Biogeosciences*, 7, 1357–1373, doi:10.5194/bg-7-1357-2010, 2010.
- Heip, C. H. R., Goosen, N. K., Herman, P. M. J., Kromkamp, J., Middelburg, J. J., and Soetaert, K.: Production and consumption of biological particles in temperate tidal estuaries, *Oceanogr. Mar. Biol.*, 33, 1–149, 1995.
- Joint, I. and Pomroy, A.: Phytoplankton biomass and production in the Southern North Sea, *Mar. Ecol.-Prog. Ser.*, 99, 169–182, 1993.
- Justic, D., Rabalais, N. N., and Turner, R. E.: Effects of climate change on hypoxia in coastal waters: a doubled CO₂ scenario for the Northern Gulf of Mexico, *Limnol. Oceanogr.*, 41, 992–1003, doi:10.4319/lo.1996.41.5.0992, 1996.
- Justić, D., Rabalais, N. N., and Turner, R. E.: Coupling between climate variability and coastal eutrophication: evidence and outlook for the Northern Gulf of Mexico, *J. Sea Res.*, 54, 25–35, doi:10.1016/j.seares.2005.02.008, 2005.
- Kaas, E. and Group, S.: Regional storm, wave and surge scenarios for the 2100 century (STOWASUS-2100), *Synthesis*, 134 ST – Regional storm, wave and surge scenarios, available at: <http://www.dmi.dk/pub/STOWASUS-2100/>, 2001.

- Keeling, R. F., Körtzinger, A., and Gruber, N.: Ocean deoxygenation in a warming world, *Ann. Rev. Mar. Sci.*, 2, 199–229, doi:10.1146/annurev.marine.010908.163855, 2010.
- Lee, J., Tett, P., Jones, K., Jones, S., Luyten, P., Smith, C., and Wild-Allen, K.: The PROWQM physical–biological model with benthic–pelagic coupling applied to the Northern North Sea, *J. Sea Res.*, 48, 287–331, 2002.
- Lowe, J. A., Howard, T. P., Pardaens, A., Tinker, J., Holt, J., Wake- lin, S., Milne, G., Leake, J., Wolf, J., Horsburgh, K., Reeder, T., Jenkins, G., Ridley, J., Dye, S., and Bradley, S.: UK Climate Projections science report: marine and coastal projections, Met Office Hadley Centre, available at: <http://ukclimateprojections.defra.gov.uk/media.jsp?mediaid=87850&filetype=pdf>, 2009.
- Luff, R. and Moll, A.: Seasonal dynamics of the North Sea sediments using a three-dimensional coupled sediment–water model system, *Cont. Shelf Res.*, 24, 1099–1127, doi:10.1016/j.csr.2004.03.010, 2004.
- Lund-Hansen, L.: Pelagic and seabed fluxes of particulate matter and carbon, and C:N ratios resolved by sediment traps during a spring bloom, Southwest Kattegat, *J. Sea Res.*, 52, 87–98, doi:10.1016/j.seares.2003.11.003, 2004.
- Marinov, I., Doney, S. C., and Lima, I. D.: Response of ocean phytoplankton community structure to climate change over the 21st century: partitioning the effects of nutrients, temperature and light, *Biogeosciences*, 7, 3941–3959, doi:10.5194/bg-7-3941-2010, 2010.
- Middelburg, J. J. and Levin, L. A.: Coastal hypoxia and sediment biogeochemistry, *Biogeosciences*, 6, 1273–1293, doi:10.5194/bg-6-1273-2009, 2009.
- Middelburg, J. J. and Soetaert, K.: The role of sediments in shelf ecosystem dynamics, in: *Respiration in Aquatic Systems*, vol. 13, edited by: Del Giorgio, P. A. and Williams, L. P. J., Oxford University Press, 353–374, 2005.
- Mills, D. K., Laane, R. W. P. M., Rees, J. M., Rutgers van der Loeff, M., Suylen, J. M., Pearce, D. J., Sivyer, D. B., Heins, C., Platt, K., and Rawlinson, M.: Smartbuoy: A marine environmental monitoring buoy with a difference, edited by: Dahlin, H., Flemming, N. C., Nittis, K., and Petersson, S.E., Elsevier Oceanography Series, Elsevier, 69, 311–316, ISSN:0422-9894, ISBN:9780444515506, doi:10.1016/S0422-9894(03)80050-8, available at: <http://www.sciencedirect.com/science/article/pii/S0422989403800508>, 2003.
- Moll, A.: Regional distribution of primary production in the North Sea simulated by a three-dimensional model, *J. Mar. Syst.*, 16, 151–170, 1998.
- Najjar, R. G., Jin, X., Louanchi, F., Aumont, O., Caldeira, K., Doney, S. C., Dutay, J. C., Follows, M., Gruber, N., Joos, F., Lindsay, K., Maier-Reimer, E., Matear, R. J., Matsumoto, K., Monfray, P., Mouchet, A., Orr, J. C., Plattner, G. K., Sarmiento, J. L., Schlitzer, R., Slater, R. D., Weirig, M. F., Yamana, Y., Yool, A.: Impact of circulation on export production, dissolved organic matter and dissolved oxygen in the ocean: Results from OCMIP-2, *Global Biogeochem. Cy.*, 21, 3007, doi:10.1029/2006GB002857, 2007.
- Neubacher, E. C., Parker, R. E., and Trimmer, M.: Short-term hypoxia alters the balance of the nitrogen cycle in coastal sediments, *Limnol. Oceanogr.*, 56, 651–665, doi:10.4319/lo.2011.56.2.0651, 2011.
- Offringa, H., Blaas, M., Stephens, M., and van den Akker, S.: Be-grenzing natuurgebieden op de Noordzee, 2004.
- Oguz, T., Ducklow, H. W., Malanotte-Rizzoli, P., Murray, J. W., Shushkina, E. A., and Vedernikov, V. I.: A physical–biochemical model of plankton productivity and nitrogen cycling in the Black Sea, *Deep Sea Res. Pt. I*, 4, 597–636, 1999.
- Osinga, R., Kop, A., and Duineveld, G.: Benthic mineralization rates at two locations in the Southern North Sea, *J. Sea Res.*, 36, 181–191, 1996.
- OSPAR: OSPAR workshop, in: 2nd OSPAR Workshop on Eutrophication Modelling, Lowestoft (UK) on 10–13 September 2007, p. 69, 2007.
- Peeters, J. C. H., Los, F. J., Jansen, R., Haas, H. A., and De Vries, I.: The oxygen dynamics of the Oyster Ground, North Sea. Impact of eutrophication and environmental conditions, *Ophelia*, 42, 257–288, doi:10.1080/00785326.1995.10431508, 1995.
- Peña, M. A., Katsev, S., Oguz, T., and Gilbert, D.: Modeling dissolved oxygen dynamics and hypoxia, *Biogeosciences*, 7, 933–957, doi:10.5194/bg-7-933-2010, 2010.
- Postma, H. and Rommets, J. W.: Variations of particulate organic carbon in the Central North Sea, *Neth. J. Sea Res.*, 18, 31–50, 1984.
- Queste, B. Y., Fernand, L., Jickells, T. D., and Heywood, K. J.: Spatial extent and historical context of North Sea oxygen depletion in August 2010, *Biogeochemistry*, doi:10.1007/s10533-012-9729-9, 2012.
- R Core Team: R: A Language and Environment for Statistical Computing, available at: <http://www.r-project.org/>, 2012.
- Rabalais, N. N., Turner, R. E., Dortch, Q., Justic, D., Bierman, V. J., and Wiseman, W. J.: Nutrient-enhanced productivity in the northern Gulf of Mexico: past, present and future, *Hydrobiologia*, 475–476, 39–63, 2002.
- Rabalais, N. N., Turner, R. E., Díaz, R. J., and Justic, D.: Global change and eutrophication of coastal waters, *ICES J. Mar. Sci.*, 66, 1528–1537, 2009.
- Rabalais, N. N., Díaz, R. J., Levin, L. A., Turner, R. E., Gilbert, D., and Zhang, J.: Dynamics and distribution of natural and human-caused hypoxia, *Biogeosciences*, 7, 585–619, doi:10.5194/bg-7-585-2010, 2010.
- Rauch, M. and Denis, L.: Spatio-temporal variability in benthic mineralization processes in the Eastern English Channel, *Biogeochemistry*, 89, 163–180, doi:10.1007/s10533-008-9191-x, 2008.
- Rauthe, M. and Paeth, H.: Relative importance of Northern Hemisphere circulation modes in predicting regional climate change, *J. Climate*, 17, 4180–4189, doi:10.1175/JCLI3140.1, 2004.
- Räisänen, J., Hansson, U., Ullerstig, A., Döscher, R., Graham, L. P., Jones, C., Meier, H. E. M., Samuelsson, P., and Willén, U.: European climate in the late twenty-first century: regional simulations with two driving global models and two forcing scenarios, *Clim. Dynam.*, 22, 13–31, 2004.
- Rockel, B. and Woth, K.: Extremes of near-surface wind speed over Europe and their future changes as estimated from an ensemble of RCM simulations, *Climatic Change*, 81, 267–280, doi:10.1007/s10584-006-9227-y, 2007.
- Ruardij, P., Van Haren, H., and Ridderinkhof, H.: The impact of thermal stratification on phytoplankton and nutrient dynamics in shelf seas: a model study, *J. Sea Res.*, 38, 311–331, doi:10.1016/S1385-1101(97)00042-7, 1997.

- Schrump, C., Alekseeva, I., and St. John, M.: Development of a coupled physical–biological ecosystem model ECOSMO, *J. Marine Syst.*, 61, 79–99, doi:10.1016/j.jmarsys.2006.01.005, 2006.
- Skogen, M. D. and Moll, A.: Interannual variability of the North Sea primary production: comparison from two model studies, *Cont. Shelf Res.*, 20, 129–151, doi:10.1016/S0278-4343(99)00069-2, 2000.
- Soetaert, K. and Herman, P. M. J.: A Practical Guide to Ecological Modelling: Using R as a Simulation Platform, edited by: Soetaert, K. and Herman, P. M. J., Springer, available at: <http://books.google.com/books?hl=en&lr=&id=aVjDtSmJqhAC&oi=fnd&pg=PA1&dq=A+practical+guide+to+ecological+modelling:+using+R+as+a+simulation+platform&ots=AJvxfEks26&sig=SjlKXYb6q0s20bguvB7Kd9i4gpM>, 2009.
- Soetaert, K. and Middelburg, J. J.: Modeling eutrophication and oligotrophication of shallow-water marine systems: the importance of sediments under stratified and well-mixed conditions, *Eutrophication in Coastal Ecosystems*, *Hydrobiologica*, 629, 239–254, doi:10.1007/s10750-009-9777-x, 2009.
- Soetaert, K., Herman, P. M. J., and Middelburg, J. J.: A model of early diagenetic processes from the shelf to abyssal depths, *Geochim. Cosmochim. Ac.*, 60, 1019–1040, 1996a.
- Soetaert, K., Herman, P. M. J., and Middelburg, J. J.: Dynamic response of deep-sea sediments to seasonal variations: a model, *Limnol. Oceanogr.*, 41, 1651–1668, doi:10.4319/lo.1996.41.8.1651, 1996b.
- Soetaert, K., Herman, P. M., Middelburg, J. J., Heip, C., Smith, C. L., Tett, P., and Wild-Allen, K.: Numerical modelling of the shelf break ecosystem: reproducing benthic and pelagic measurements, *Deep-Sea Res. Pt. II*, 48, 3141–3177, doi:10.1016/S0967-0645(01)00035-2, 2001.
- Soetaert, K., Petzoldt, T., and Setzer, R. W.: Solving differential equations in R: package desolve, *J. Stat. Soft.*, 33, 1–25, 2010.
- Sterl, A., van den Brink, H., de Vries, H., Haarsma, R., and van Meijgaard, E.: An ensemble study of extreme storm surge related water levels in the North Sea in a changing climate, *Ocean Sci.*, 5, 369–378, doi:10.5194/os-5-369-2009, 2009.
- Suratman, S., Jickells, T., Weston, K., and Fernand, L.: Seasonal variability of inorganic and organic nitrogen in the North Sea, *Hydrobiologia*, 610, 83–98, doi:10.1007/s10750-008-9424-y, 2008.
- Upton, A. C., Nedwell, D. B., Parkes, R. J., and Harvey, S. M.: Seasonal benthic microbial activity in the Southern North Sea; oxygen uptake and sulphate reduction, *Mar. Ecol.-Prog. Ser.*, 101, 273–281, doi:10.3354/meps101273, 1993.
- van der Molen, J.: The influence of tides, wind and waves on the net sand transport in the North Sea, *Cont. Shelf Res.*, 22, 2739–2762, doi:10.1016/S0278-4343(02)00124-3, 2002.
- Vaquier-Sunyer, R. and Duarte, C. M.: Thresholds of hypoxia for marine biodiversity, *P. Natl. Acad. Sci. USA*, 105, 15452–15457, doi:10.1073/pnas.0803833105, 2008.
- Vermaat, J. E., McQuatters-Gollop, A., Eleveld, M. A., and Gilbert, A. J.: Past, present and future nutrient loads of the North Sea: causes and consequences, *Estuar. Coast. Shelf S.*, 80, 53–59, doi:10.1016/j.ecss.2008.07.005, 2008.
- Wanninkhof, R. and McGillis, W. R.: A cubic relationship between air–sea CO₂ exchange and wind speed, *Geophys. Res. Lett.*, 26, 1889–1892, 1999.
- Weston, K., Fernand, L., Nicholls, J., Marca-Bell, A., Mills, D., Sivyer, D., and Trimmer, M.: Sedimentary and water column processes in the Oyster Grounds: a potentially hypoxic region of the North Sea, *Mar. Environ. Res.*, 65, 235–49, doi:10.1016/j.marenvres.2007.11.002, 2008.
- Woth, K., Weisse, R., and Storch, H.: Climate change and North Sea storm surge extremes: an ensemble study of storm surge extremes expected in a changed climate projected by four different regional climate models, *Ocean Dynam.*, 56, 3–15, doi:10.1007/s10236-005-0024-3, 2005.
- Young, I. R., Zieger, S., and Babanin, A. V.: Global trends in wind speed and wave height, *Science*, 332, 451–455, 2011.
- Zhang, J., Gilbert, D., Gooday, A. J., Levin, L., Naqvi, S. W. A., Middelburg, J. J., Scranton, M., Ekau, W., Peña, A., Dewitte, B., Oguz, T., Monteiro, P. M. S., Urban, E., Rabalais, N. N., Ittekkot, V., Kemp, W. M., Ulloa, O., Elmgren, R., Escobar-Briones, E., and Van der Plas, A. K.: Natural and human-induced hypoxia and consequences for coastal areas: synthesis and future development, *Biogeosciences*, 7, 1443–1467, doi:10.5194/bg-7-1443-2010, 2010.